Photonic-Fock-state scattering in a waveguide-QED system and their correlation functions

Yuecheng Shen and Jung-Tsung Shen*

Department of Electrical and Systems Engineering, Washington University in St. Louis, St. Louis, Missouri 63130, USA

(Received 20 May 2015; published 2 September 2015)

We investigate the problem of arbitrary photonic-Fock-state scattering in a waveguide-QED system which consists of a one-dimensional waveguide coupled to a two-level system. By imposing the open boundary conditions that directly describe the physical settings, we construct a complete set of eigenstates of the system, and elucidate the mathematical structures of the eigenstates. In particular, we show that the eigenstates include a set of multiphoton extended states and multiphoton bound states, formed by all possible partitions of the photon number N. The total number of the eigenstates is exactly described by the integer number partition function $Z(N)$. Using the set of eigenstates, we form the scattering matrix, which facilitates the calculations of the scattered photon states, for the scattering processes. With the scattered photon states, we compute the photon correlation functions that manifestly exhibit the bunching and antibunching behaviors in the scattered photon states. As a concrete example, we discuss in detail with a focus on the three-photon Fock state. Such a capability to generate photonic entanglement from unentangled Fock states will have broad applications in quantum information processing.

DOI: 10.1103/PhysRevA.92.033803 PACS number(s): 42.50.Pq, 32.80.−t, 03.65.Nk, 72.10.Fk

I. INTRODUCTION

There has been greatly growing interest in engineering the photon correlations in photonic Fock states, which are multiphoton states of a traveling wave packet that contains a definite number of photons and is characterized by a temporal or spectral profile. This interest stems partly from the advent of the experimental capability of controlled generation of multiphoton Fock states in a solid-state system (the photon number $N \leqslant 6$ in current experiments [1]). When the photonic wave function of the Fock state is not a product state of the wave functions of the constituent individual photons, the photons are entangled. We call such states entangled photonic Fock states. Entangled photonic Fock states are potentially useful in many applications. For example, entangled N-photon bound states, of which the wave function decays exponentially when the relative distance between any pair of photons increases, could exhibit photonic bunching and an effective wavelength that is N times smaller than that of individual photons [2]. Such entangled states could achieve deep subwavelength optical lithography [3,4] and super resolution in optical imaging [5,6]. On the other hand, entangled photonic Fock states which exhibit antibunching behavior and sub-Possionian statistics provide ultraquiet photon sources with sub-shot-noise power level and also make possible single-photon sources for quantum information processing [7,8]. Nonetheless, a comprehensive theoretical description in solid-state quantum electrodynamics (QED) systems on how the photon entanglement emerges in photonic Fock states by scattering means has not been presented before. One of the sources of difficulty is the proper treatment of the boundary conditions in an infinite system for the optical fields of interest. Conventionally, a periodic or hard-wall boundary condition has been employed to truncate the system size to make the computation region finite. Although computationally convenient, those boundary conditions do not describe the correct physical settings in an infinite physical system. Furthermore, due to the mathematical complexity, the exact solutions of the scattering problems were postulated using the Bethe ansatz [9], instead of being derived directly. Not until very recently, have approaches using open boundary conditions been employed to investigate the two-photon Fock-state scattering problems [10,11]. These approaches do not assume the Bethe anstaz as *a priori* assumptions. However, the direct generalizations of these approaches to describe the N-photon Fock-state ($N > 2$) scattering problems are subtle, mainly due to the emergence of multiple photonic threshold bound states [12]. In this study, we provide a detailed investigation for the N-photon Fock-state scattering problems in a waveguide-QED system which consists of a one-dimensional waveguide coupled to a two-level atom. Such a system provides the simplest realization for the photon-atom interactions in waveguide-QED systems. Notably, the fermionic degree of freedom in the atom induces interplay between the photons, which fundamentally changes the collective photon transport properties. Specifically, without relying on any ansatz, we employ the open boundary conditions to solve the N-photon Fock-state scattering processes by explicitly constructing a complete set of eigenstates of the system. The constructed eigenstates contain very rich mathematical structures. For instance, for the three-photon Fock state, there are in total three types of eigenstates with different physical nature: a three-photon extended state, a three-photon threshold bound state, and a hybrid state that is linear superposition of a three-photon bound state and a product state of a two-bound state and an extended state. For the general case of the N-photon Fock state, we show that the total number of different types of eigenstates is exactly described by the integer number partition function $Z(N)$; the set of eigenstates in general includes hybrid states of multiphoton extended states and multiphoton threshold bound states, formed by all possible partitions of the photon number N. Physically, the N-photon threshold bound states would give rise to N-photon bunching behavior that is mathematically characterized by the Nth-order correlation function. To construct the scattering matrix, which encodes all the information of the scattering process, it is vital that the sets of in states and out states that are obtained from the set of eigenstates are complete in the free space, respectively.

*jushen@wustl.edu

For this purpose, we develop a numerical scheme to check this property. Finally, as a concrete example, we consider the case of the three-photon Fock state, and compute the third-order correlation function to demonstrate the bunching and antibunching behaviors in the scattered photon states. Those nontrivial bunching and antibunching behaviors are closely related to the existence of the threshold bound states.

The article is organized as follows. In Sec. II, we introduce the Hamiltonian of the waveguide-QED system, which is said to be nonchiral. For mathematical convenience, this to be solved nonchiral Hamiltonian can be decomposed into two decoupled chiral Hamiltonians. In Sec. III, we present the solutions for the chiral systems including the eigenstates, in states, and out states, and discuss their properties for different photon number N. Then, Sec. IV shows how to construct the scattering matrix in the nonchiral system by using the solved solutions in the chiral systems. In Secs. V and VI, as a concrete example, we numerically compute the scattered three-photon Fock state in the nonchiral system, and discuss the photonic wave functions and correlation functions in detail. Finally, we make our conclusions in Sec. VII. Detailed mathematical derivations are presented in the Appendixes.

II. THE HAMILTONIAN FOR A WAVEGUIDE-QED SYSTEM

The system of interest is depicted in Fig. 1, which consists of a one-dimensional waveguide coupled to a two-level system. The two-level system can be a quantum dot [13,14], a superconducting qubit [15,16], a nitrogen vacancy center [17], or an atom [18,19], and hereafter is referred to as "an atom"; the one-dimensional waveguide, for example, can be a line-defect waveguide in a photonic crystal [20] or an optical fiber. To have a robust realization of such a waveguide-QED system, it is required to have a sufficiently large β factor [21,22], which describes the spontaneous emission efficiency into the waveguide. Furthermore, the waveguide is a single-polarization single-mode (SPSM) waveguide [23], so that there would be no photonic mode conversions that degrade the interference [24]. The Hamiltonian of the entire waveguide-QED system can be described by a real-space form (for detailed derivation from the frequency-space form, see Ref. [25])

$$\begin{aligned} H/\hbar = &\int dx(-i)vC_R^\dagger(x)\frac{\partial}{\partial x}C_R(x) + \int dx\, ivC_L^\dagger(x)\frac{\partial}{\partial x}C_L(x) \\ &+ \int dx\bar{V}\delta(x)[C_R^\dagger(x)\sigma_- + C_R(x)\sigma_+ + C_L^\dagger(x)\sigma_- \\ &+ C_L(x)\sigma_+] + \omega_e a_e^\dagger a_e + \omega_g a_g^\dagger a_g. \end{aligned} \tag{1}$$

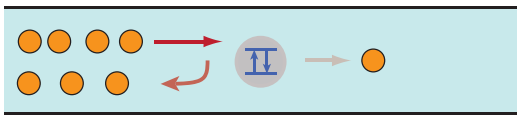

FIG. 1. (Color online) Schematics of the described system. A one-dimensional waveguide is coupled to a two-level atom. Multiple photons are incident from the left side and are scattered by the two-level atom. Each photon can be either reflected or transmitted after scattering.

Here, v is the group velocity of the photons in the waveguide. $C_R^\dagger(x)$ and $C_R(x)$ [$C_L^\dagger(x)$ and $C_L(x)$] are the operators that create and annihilate a right- (left-) moving photon at position x. Here, for brevity, the polarization and mode indices for the photons in the SPSM waveguide are suppressed. $a_e^\dagger$ and a_e ($a_g^\dagger$ and a_g) are the creation and annihilation operators of the excited (ground) state of the atom. Thus, $\sigma_+ \equiv a_e^\dagger a_g$ and $\sigma_- \equiv a_g^\dagger a_e$ are the ladder operators that excite and deexcite the atom, respectively. $\hbar\omega_e$ and $\hbar\omega_g$ are the energy levels of the atom in the excited state and the ground state. $\bar{V}$ is the coupling constant between the waveguide and the atom ($\Gamma \equiv 2\bar{V}^2/v$ is the spontaneous emission rate in the waveguide and also characterizes the width of the transmission spectrum [24]). Hereafter, the system which is described by such a Hamiltonian is said to be nonchiral, wherein photons can propagate in both directions.

For an N-photon Fock-state scattering process in the nonchiral system, a direct attempt to solve for the eigenstates is mathematically complicated, as one has to deal with a plethora of all possible transmitted and reflected states, which involves $2^N N!$ independent parameters to be determined. Instead, to ease the calculation complexity, an efficient strategy is to first solve the n-photon scattering process in the chiral space for $n = 1,2,\ldots,N$, wherein photons only propagate in one direction. Then, the solutions in the chiral space with different photon numbers n are recombined to construct the solutions in the nonchiral space [11]. To go from the nonchiral Hamiltonian to the chiral ones, we perform the following transformations:

$$\begin{aligned} C_e^\dagger(x) &\equiv \frac{1}{\sqrt{2}}[C_R^\dagger(x) + C_L^\dagger(-x)], \\ C_o^\dagger(x) &\equiv \frac{1}{\sqrt{2}}[C_R^\dagger(x) - C_L^\dagger(-x)], \end{aligned} \tag{2}$$

to decompose the Hamiltonian into two decoupled even and odd parts ($H = H_e + H_o$):

$$\begin{aligned} H_e/\hbar = &\int dx(-i)vC_e^\dagger(x)\frac{\partial}{\partial x}C_e(x) + \int dx V\delta(x) \\ &\times [C_e^\dagger(x)\sigma_- + C_e(x)\sigma_+] + \omega_e a_e^\dagger a_e + \omega_g a_g^\dagger a_g, \\ H_o/\hbar = &\int dx(-i)vC_o^\dagger(x)\frac{\partial}{\partial x}C_o(x), \end{aligned} \tag{3}$$

where $[H_e, H_o] = 0$. Here, H_o is an interaction-free Hamiltonian, while H_e includes the interaction with an effective coupling strength $V \equiv \sqrt{2}\bar{V}$. The systems described by the Hamiltonians H_e and H_o are referred to as the chiral systems with unidirectional propagation of photons. Mathematically, a complete set of solutions for both chiral systems allows one to solve the scattering problems in the corresponding nonchiral system. Although the chiral systems here described by Eq. (3) are for mathematical convenience, there are physical systems which are precisely described by the chiral Hamiltonians, such as the photonic analog of the quantum Hall effect [26,27]. In those chiral systems, the backscattered modes are completely suppressed. Thus, the chiral systems are anticipated to be robust for structural imperfections and slow light operations. In view of these possibilities, we present the investigations for the chiral systems in the next section.

III. THE SOLUTIONS FOR THE CHIRAL SYSTEM

An N-photon interacting eigenstate $|i^+\rangle$ of the chiral system described by H_e satisfies $H_e|i^+\rangle = E|i^+\rangle$ and is defined in the Hilbert space $\mathcal{H}_e^{\otimes N}$, where $\mathcal{H}_e$ is the one-photon Hilbert space. $|i^+\rangle$ has the following general form:

$$\begin{aligned}|i^+\rangle = &\int\cdots\int dx_1dx_2\cdots dx_N f(x_1,x_2,\ldots,x_N)\\ &\times\frac{1}{\sqrt{N!}}C_e^\dagger(x_1)C_e^\dagger(x_2)\cdots C_e^\dagger(x_N)|\emptyset,-\rangle\\ &+\int\cdots\int dx_1dx_2\cdots dx_{N-1}e(x_1,x_2,\ldots,x_{N-1})\\ &\times\frac{1}{\sqrt{(N-1)!}}C_e^\dagger(x_1)C_e^\dagger(x_2)\cdots C_e^\dagger(x_{N-1})\sigma_+|\emptyset,-\rangle,\end{aligned} \tag{4}$$

where $|\emptyset,-\rangle$ is the vacuum state with zero photon in the waveguide and the atom in the ground state. The first term corresponds to the situation that the atom is in the ground state and the N photons are in the waveguide described by an N-photon wave function $f(x_1,x_2,\ldots,x_N)$. The second term, on the other hand, corresponds to the situation when one of the N photons is absorbed by the atom and the atom is in the excited state. The other $N-1$ photons in the waveguide are described by an $(N-1)$-photon wave function $e(x_1,x_2,\ldots,x_{N-1})$. The prefactors $1/\sqrt{N!}$ and $1/\sqrt{(N-1)!}$ are the normalization constants [28]. Due to the bosonic nature of the photons, photonic wave functions $f(x_1,x_2,\ldots,x_N)$ and $e(x_1,x_2,\ldots,x_{N-1})$ have the exchange symmetric with respect to the exchange of any two coordinates.

From the Schrödinger equation $H_e|i^+\rangle = E|i^+\rangle$, by equating the coefficients for each basis, we obtain the equations of motion as follows:

$$\begin{aligned}&\left[-iv\frac{\partial}{\partial x_1}-iv\frac{\partial}{\partial x_2}-\cdots-iv\frac{\partial}{\partial x_N}-E/\hbar\right]f(x_1,x_2,\ldots,x_N)\\ &\quad+\frac{V}{\sqrt{N}}[\delta(x_1)e(x_2,x_3,\ldots,x_N)+\delta(x_2)e(x_1,x_3,\ldots,x_N)+\cdots+\delta(x_N)e(x_1,x_2,\ldots,x_{N-1})]=0,\end{aligned} \tag{5}$$

$$\begin{aligned}&\left[-iv\frac{\partial}{\partial x_1}-iv\frac{\partial}{\partial x_2}-\cdots-iv\frac{\partial}{\partial x_{N-1}}-(E/\hbar-\Omega)\right]e(x_1,x_2,\ldots,x_{N-1})\\ &\quad+\frac{V}{\sqrt{N}}[f(0,x_1,x_2,\ldots,x_{N-1})+f(x_1,0,x_2,\ldots,x_{N-1})+\cdots+f(x_1,x_2,\ldots,x_{N-1},0)]=0,\end{aligned} \tag{6}$$

where $\Omega\equiv\omega_e-\omega_g$ is the transition frequency of the atom. From Eqs. (5) and (6), all the possible solutions of $f(x_1,x_2,\ldots,x_N)$ and $e(x_1,x_2,\ldots,x_{N-1})$ can be solved for (see Appendix A), which provide a complete set of interacting eigenstates $\{|i^+\rangle\}$. By using the Lippmann-Schwinger equation [29], the solved set of eigenstates $|i^+\rangle$ can be used to obtain the corresponding in states $|\text{in}\rangle$ and out states $|\text{out}\rangle$ [11]:

$$\begin{aligned}|\text{in}\rangle &= \int\cdots\int dx_1dx_2\cdots dx_N f_{\text{in}}(x_1,x_2,\ldots,x_N)\frac{1}{\sqrt{N!}}C_e^\dagger(x_1)C_e^\dagger(x_2)\cdots C_e^\dagger(x_N)|\emptyset,-\rangle,\\ |\text{out}\rangle &= \int\cdots\int dx_1dx_2\cdots dx_N f_{\text{out}}(x_1,x_2,\ldots,x_N)\frac{1}{\sqrt{N!}}C_e^\dagger(x_1)C_e^\dagger(x_2)\cdots C_e^\dagger(x_N)|\emptyset,-\rangle.\end{aligned} \tag{7}$$

The in-state wave function $f_{\text{in}}(x_1,x_2,\ldots,x_N)$ is the extension of the eigenstate wave function,

$$f_{\text{in}}(x_1,\ldots,x_N)\equiv\text{Ext}[f(x_1<0,\ldots,x_N<0)]. \tag{8}$$

This equation means that the functional form of $f_{\text{in}}(x_1,\ldots,x_N)$ is the same as that of $f(x_1,\ldots,x_N)$ in the restricted region $x_1<0,\ldots,x_N<0$, but all arguments are extended to the entire space so that now $-\infty<x_j<\infty$ for all j [30]. Similarly, the out-state wave function $f_{\text{out}}(x_1,x_2,\ldots,x_N)$ is the extension of the eigenstate wave function:

$$f_{\text{out}}(x_1,\ldots,x_N)\equiv\text{Ext}[f(x_1>0,\ldots,x_N>0)]. \tag{9}$$

Both the in states and the out states are *free* states that are governed by the free Hamiltonian. For each in state, there exists a causally related out state. The in states and out states are complete in the in and out spaces, respectively. With the full knowledge of the in states and out states, one can construct the scattering matrix for any states $\in\mathcal{H}_e^{\otimes N}$,

$$\mathbf{S}_{e^{(N)}}=\sum_{\{|\text{in}\rangle\}}|\text{out}\rangle\langle\text{in}|, \tag{10}$$

which maps a free N-photon Hilbert space of in states to another free N-photon Hilbert space consisting of out states. The summation is taken over for a complete basis $\{|\text{in}\rangle\}$. Once the scattering matrix is determined, one can calculate the output state of the system for an arbitrary input state when the atom is initially in the ground state.

In the following, we show explicitly the form of the complete set of the in states for different photon numbers from $N=1$ to 4, as well as the general case N.

(1) One-photon case: For this simplest case, the class of the in-state wave functions can be represented by a plane wave,

$$f_{\text{in}}(x)=C_1e^{ikx}, \tag{11}$$

TABLE I. Two-photon in-state classifications.

Type 1	k_1, k_2 (real numbers)	(1,1)
Type 2	$k_1 = k - i\Gamma/(2v), k_2 = k + i\Gamma/(2v)$	(2)

which is characterized by a single real parameter $k = E/(v\hbar) \in \mathbb{R}$. For different k, these waves form a complete set. C_1 is the normalization constant, which can be determined using the normalization condition detailed in Appendix B.

(2) Two-photon case: The general form of the class of in-state wave functions is

$$f_{\rm in}(x_1,x_2) = C_2\{[k_1 - k_2 - i\Gamma\,\mathrm{sgn}(x_2 - x_1)/v]e^{ik_1x_1+ik_2x_2} + [k_1 - k_2 - i\Gamma\,\mathrm{sgn}(x_1 - x_2)/v]e^{ik_2x_1+ik_1x_2}\}, \tag{12}$$

where $\mathrm{sgn}(\cdot)$ is the sign function with $\mathrm{sgn}(x > 0) = 1$ and $\mathrm{sgn}(x < 0) = -1$. $\Gamma = 2\bar{V}^2/v = V^2/v$ is the spontaneous emission rate into the waveguide. k_1 and k_2 are in general two complex numbers subject to the constraint of $k_1 + k_2 = E/(v\hbar) \in \mathbb{R}$, among others. Such a constraint imposes that either both k_1 and k_2 are real (type 1) or their imaginary parts have an opposite sign (type 2). A full analysis shows that in type 2, k_1 and k_2 are in fact complex conjugate to each other (i.e., have the same real part). In general, these two types of in states exhibit different forms of wave functions, thereby requiring different normalization constants (Appendix B). Table I summarizes the properties of the two types of in states.

TABLE II. Three-photon in-state classifications.

Type 1	k_1, k_2, k_3 (real numbers)	(1,1,1)
Type 2	$k_1 = k - i\Gamma/(2v), k_2 = k + i\Gamma/(2v), k_3$	(2,1)
Type 3	$k_1 = k - i\Gamma/v, k_2 = k, k_3 = k + i\Gamma/v$	(3)

In type 1, both k_1 and k_2 are real, which leads to a two-photon extended state. In type 2, $k_1 = k - i\Gamma/(2v)$ and $k_2 = k + i\Gamma/(2v)$, where $k = E/(2v\hbar)$, so that the wave function can be further reduced to

$$f_{\rm in}(x_1,x_2) = C_2 e^{ik(x_1+x_2)-|x_2-x_1|\Gamma/(2v)}. \tag{13}$$

This wave function describes a two-photon bound state, as the wave function approaches to zero exponentially when the two photons become far. It has been shown that these two types of in states form a complete set in the two-photon Hilbert space [11]. In the last column of the table, we also list all possible partitions of the photon number $N = 2$. The assigning rule is as follows: for unrestricted real number E, if a single variable can specify the values of j k's, a number j is assigned in the column. For the present case, in type 1, k_1 and k_2 need to be independently specified, so this type is assigned (1,1). In type 2, a single variable k can specify the values of both k_1 and k_2 (Γ and v are given constants), thus (2) is assigned in the column.

(3) Three-photon case: The general form of the class of in-state wave functions is

$$\begin{aligned} f_{\rm in}(x_1,x_2,x_3) = C_3\{&[k_1 - k_2 - i\Gamma\,\mathrm{sgn}(x_2 - x_1)/v][k_2 - k_3 - i\Gamma\,\mathrm{sgn}(x_3 - x_2)/v][k_1 - k_3 - i\Gamma\,\mathrm{sgn}(x_3 - x_1)/v]e^{i(k_1x_1+k_2x_2+k_3x_3)} \\ &+ [k_1 - k_2 - i\Gamma\,\mathrm{sgn}(x_3 - x_1)/v][k_2 - k_3 - i\Gamma\,\mathrm{sgn}(x_2 - x_3)/v][k_1 - k_3 - i\Gamma\,\mathrm{sgn}(x_2 - x_1)/v]e^{i(k_1x_1+k_2x_3+k_3x_2)} \\ &+ [k_1 - k_2 - i\Gamma\,\mathrm{sgn}(x_1 - x_2)/v][k_2 - k_3 - i\Gamma\,\mathrm{sgn}(x_3 - x_1)/v][k_1 - k_3 - i\Gamma\,\mathrm{sgn}(x_3 - x_2)/v]e^{i(k_1x_2+k_2x_1+k_3x_3)} \\ &+ [k_1 - k_2 - i\Gamma\,\mathrm{sgn}(x_1 - x_3)/v][k_2 - k_3 - i\Gamma\,\mathrm{sgn}(x_2 - x_1)/v][k_1 - k_3 - i\Gamma\,\mathrm{sgn}(x_2 - x_3)/v]e^{i(k_1x_3+k_2x_1+k_3x_2)} \\ &+ [k_1 - k_2 - i\Gamma\,\mathrm{sgn}(x_3 - x_2)/v][k_2 - k_3 - i\Gamma\,\mathrm{sgn}(x_1 - x_3)/v][k_1 - k_3 - i\Gamma\,\mathrm{sgn}(x_1 - x_2)/v]e^{i(k_1x_2+k_2x_3+k_3x_1)} \\ &+ [k_1 - k_2 - i\Gamma\,\mathrm{sgn}(x_2 - x_3)/v][k_2 - k_3 - i\Gamma\,\mathrm{sgn}(x_1 - x_2)/v][k_1 - k_3 - i\Gamma\,\mathrm{sgn}(x_1 - x_3)/v]e^{i(k_1x_3+k_2x_2+k_3x_1)}\}, \end{aligned} \tag{14}$$

where k_1, k_2, and k_3 are in general complex numbers subject to the constraint of $k_1 + k_2 + k_3 = E/(v\hbar)$. In such a three-photon Hilbert space, there are in total three different types of in states, illustrated in Table II.

In type 1, k_1, k_2, and k_3 are three independent real numbers, which leads to a three-photon extended state and is assigned (1,1,1). In type 2, $k_1 = k - i\Gamma/(2v)$ and $k_2 = k + i\Gamma/(2v)$ are complex conjugate to each other, while the third number k_3 is a real number. This type is accordingly assigned (2,1). To gain insights for the mathematical structure of this wave function, we focus on a specific region, e.g., $x_1 < x_2 < x_3$, to remove all the sign functions,

$$\begin{aligned} f_{\rm in}(x_1,x_2,x_3) = C_3\{&[k - k_3 - i\Gamma/(2v)][k - k_3 - i3\Gamma/(2v)]e^{ik(x_1+x_2)+ik_3x_3-(x_2-x_1)\Gamma/(2v)} \\ &+ [k - k_3 + i3\Gamma/(2v)][k - k_3 - i3\Gamma/(2v)]e^{ik(x_1+x_3)+ik_3x_2-(x_3-x_1)\Gamma/(2v)} \\ &+ [k - k_3 + i3\Gamma/(2v)][k - k_3 + i\Gamma/(2v)]e^{ik(x_2+x_3)+ik_3x_1-(x_3-x_2)\Gamma/(2v)}\}. \end{aligned} \tag{15}$$

In such a wave function, the first term and the third term indicate one two-photon bound state and one one-photon extended state. The second term in the wave function, however, describes the situation that all three photons are bounded, as the coordinates are in the region of $x_1 < x_2 < x_3$. The wave function in the other five regions can be obtained straightforwardly using the exchange symmetry with respect to the coordinates. Finally, in type 3, $k_1 = k - i\Gamma/v$, $k_2 = k$, and $k_3 = k + i\Gamma/v$, and the wave function is reduced to

$$f_{\rm in}(x_1,x_2,x_3) = C_3 e^{ik(x_1+x_2+x_3)-(|x_3-x_1|+|x_2-x_1|+|x_3-x_2|)\Gamma/(2v)}. \tag{16}$$

TABLE III. Four-photon in-state classifications.

Type 1	k_1, k_2, k_3, k_4 (real numbers)	(1,1,1,1)
Type 2	$k_1 = k - i\Gamma/(2v), k_2 = k + i\Gamma/(2v), k_3, k_4$	(2,1,1)
Type 3	$k_1 = k - i\Gamma/(2v), k_2 = k + i\Gamma/(2v)\ k_3 = k' - i\Gamma/(2v), k_4 = k' + i\Gamma/(2v)$	(2,2)
Type 4	$k_1 = k - i\Gamma/v, k_2 = k, k_3 = k + i\Gamma/v, k_4$	(3,1)
Type 5	$k_1 = k - 3i\Gamma/(2v), k_2 = k - i\Gamma/(2v), k_3 = k + i\Gamma/(2v), k_4 = k + 3i\Gamma/(2v)$	(4)

Such a wave function describes a three-photon bound state, as the wave function approaches to zero exponentially when any two of the three photons become afar. For all three types of in states, we develop a computational procedure to check the completeness of these three types of in states, which is detailed in Appendix C.

(4) Four-photon case: Analogous to the previous case, the complete set of in states for the $N = 4$ case can be classified into five different types, illustrated in Table III.

(5) N-photon case: The general form of the class of in-state wave functions is

$$f_{\rm in}(x_1,x_2,\ldots,x_N) = C_N \sum_{\mathcal{P}\in S_N} \left\{ \prod_{m<n} [k_m - k_n - i\Gamma\ \ {\rm sgn}(x_{\mathcal{P}_n} - x_{\mathcal{P}_m})/v] \right\} \times \exp\left(i \sum_{j=1}^{N} k_j x_{\mathcal{P}_j} \right), \tag{17}$$

where S_N is the symmetric group on an N-element set $\{1,2,\ldots,N\}$, and the summation $\mathcal{P} \in S_N$ accounts for all the $N!$ permutations of the labels $\{1,2,\ldots,N\}$. $k_1, k_2, \ldots,$ and k_N are in general N complex numbers subject to the constraint of $k_1 + k_2 + \cdots + k_N = E/(v\hbar)$. We note that Eq. (17) satisfies the form of Bethe ansatz [31]. In the N-photon Hilbert space, the total number of types of in states is exactly the partition function $Z(N)$ for an integer number N. The first ten values of $Z(N)$ are 1,2,3,5,7,11,15,22,30,42. For large values of N, $Z(N)$ increases exponentially with an asymptotic behavior given by [32]

$$Z(N) \sim \frac{1}{4N\sqrt{3}} e^{\pi\sqrt{2N/3}}. \tag{18}$$

Table IV classifies all types of in states for the N-photon case. We note that all the values of k in each type are in agreement with that obtained using the Bethe anstaz approach [9].

In type 1, all the $k_1, k_2, \ldots,$ and k_N are real numbers, which leads to an N-photon extended state and is assigned $(1,1,\ldots,1,1)$. In type 2, $k_1 = k - i\Gamma/(2v)$ and $k_2 = k + i\Gamma/(2v)$ are complex conjugate to each other, while the remaining $N-2$ k's are independent real variables. For simplicity, we focus on a specific region $x_1 < x_2 < \cdots < x_N$ to remove all the sign functions. A direct substitution of the k's into Eq. (17) reveals that half of terms in the wave function vanish as their coefficients become zero, and only half of the terms remain. Among the remaining terms, for coordinates x_l and x_m $(l < m)$ paired with the two complex conjugates $k_1 = k - i\Gamma/(2v)$ and $k_2 = k + i\Gamma/(2v)$, such term would give rise to a form of $e^{-(x_m - x_l)\Gamma/(2v)}$. As $x_1 < x_2 < \cdots < x_N$, the $m - l + 1$ photons with coordinates $x_l, \ldots, x_m$ form an $(m - l + 1)$-photon bound state. The rest of $(N - m + l - 1)$ photons form an $(N - m + l - 1)$-photon extended state. The type $Z(N)$ has N complex k's: $k_j = k + [2j - (N + 1)]\Gamma/(2v)$, $j = 1,2,\ldots,N$. By substituting them into Eq. (17), the wave function is reduced to

$$f_{\rm in}(x_1,x_2,\ldots,x_N) = C_N e^{ik(x_1+x_2+\cdots+x_N) - (\sum_{m<n}|x_m - x_n|)\Gamma/(2v)}, \tag{19}$$

which only contains one term, describing an N-photon bound state, as the wave function approaches zero exponentially when any two of the N photons become afar. The concept of multiphoton bound states has also been discussed by Zheng *et al.* [33]. Nonetheless, the wave functions presented there are not correct.

Having introduced all possible in-state wave functions, the out-state wave functions can be expressed by multiplying an N-photon transmission amplitude to the in-state wave functions (see Aappendix A for details):

$$f_{\rm out}(x_1,x_2,\ldots,x_N) = T(k_1,k_2,\ldots,k_N) f_{\rm in}(x_1,x_2,\ldots,x_N), \tag{20}$$

where

$$T(k_1,k_2,\ldots,k_N) = \prod_{k_j} t_{k_j}, \tag{21}$$

and

$$t_{k_j} \equiv \frac{k_j - \Omega/v - i\Gamma/(2v)}{k_j - \Omega/v + i\Gamma/(2v)} \tag{22}$$

is the single-photon transmission amplitude in the chiral system with absolute value equal to one. With all the

TABLE IV. N-photon in-state classifications.

Type 1	$k_1, \ldots, k_N$ (real numbers)	$(1,1,\ldots,1,1)$
Type 2	$k_1 = k - i\Gamma/(2v), k_2 = k + i\Gamma/(2v), k_3, \ldots, k_N$	$(2,1,\ldots,1)$
...	...	...
Type $Z(N)$	$k_1 = k - i(N-1)\Gamma/(2v), k_2 = k - i(N-3)\Gamma/(2v),$	
	$\vdots$	
	$k_{N-1} = k + i(N-3)\Gamma/(2v), k_N = k + i(N-1)\Gamma/(2v)$	(N)

in states and out states, the scattering matrix for Hamiltonian H_e is formed using the definition in Eq. (10). The scattering matrix for Hamiltonian H_o, on the other hand, is simply an identity matrix. We note that in the above procedure, the in states thus constructed are eigenstates of the scattering matrix, which encodes the optical nonlinearity induced by the atomic degree of freedom.

IV. THE SCATTERING MATRIX FOR NONCHIRAL SYSTEM

Having solved the scattering problems for the chiral case, we now compute the scattered photon states for the nonchiral systems, wherein the photons can propagate in both directions. For the nonchiral case, a typical input Fock state $|X_{\rm in}\rangle$ that contains N right-moving photons can be written as

$$\begin{aligned}|X_{\rm in}\rangle &= \int\cdots\int dx_1dx_2\cdots dx_N h(x_1,x_2,\ldots,x_N)\frac{1}{\sqrt{N!}}C_R^\dagger(x_1)C_R^\dagger(x_2)\cdots C_R^\dagger(x_N)|\emptyset,-\rangle\\ &= \int\cdots\int dx_1dx_2\cdots dx_N h(x_1,x_2,\ldots,x_N)\frac{1}{\sqrt{N!}}\left(\frac{1}{\sqrt{2}}\right)^N[C_e^\dagger(x_1)+C_o^\dagger(x_1)]\cdots[C_e^\dagger(x_N)+C_o^\dagger(x_N)]|\emptyset,-\rangle\\ &= \int\cdots\int dx_1dx_2\cdots dx_N h(x_1,x_2,\ldots,x_N)\frac{1}{\sqrt{N!}}\left(\frac{1}{\sqrt{2}}\right)^N C_e^\dagger(x_1)\cdots C_e^\dagger(x_N)|\emptyset,-\rangle+\cdots\\ &\quad+\int\cdots\int dx_1dx_2\cdots dx_N h(x_1,x_2,\ldots,x_N)\frac{1}{\sqrt{N!}}\left(\frac{1}{\sqrt{2}}\right)^N C_o^\dagger(x_1)\cdots C_o^\dagger(x_N)|\emptyset,-\rangle.\end{aligned}\tag{23}$$

Here, $h(x_1,x_2,\ldots,x_N)$ is the N-photon wave function. In the second equality, we have used the inverse relation of Eq. (2). For an input Fock state that contains N left-moving photons, the process will proceed similarly. In the last equality, the direct expansion gives rise to 2^N terms. Since $C_e^\dagger(x)$ and $C_o^\dagger(x)$ commute, using the exchange symmetry with respect to the coordinates in the wave function, these 2^N terms can be grouped into $N+1$ orthogonal terms. Thus, $|X_{\rm in}\rangle$ can be written as a linear superposition of $N+1$ chiral spaces.

$$|X_{\rm in}\rangle = |X_{\rm in}\rangle_{e^{(N)}} + |X_{\rm in}\rangle_{e^{(N-1)}o^{(1)}} + \cdots + |X_{\rm in}\rangle_{o^{(N)}}.\tag{24}$$

Here, $|X_{\rm in}\rangle_{e^{(j)}o^{(N-j)}}$ is given by

$$|X_{\rm in}\rangle_{e^{(j)}o^{(N-j)}} = \int\cdots\int dx_1dx_2\cdots dx_N h(x_1,x_2,\ldots,x_N)\frac{1}{\sqrt{N!}}\left(\frac{1}{\sqrt{2}}\right)^N\frac{N!}{j!(N-j!)}C_e^\dagger(x_1)\cdots C_e^\dagger(x_j)C_o^\dagger(x_{j+1})\cdots C_o^\dagger(x_N)|\emptyset,-\rangle,\tag{25}$$

which describes a state in the $e^{(j)}o^{(N-j)}$ space where j photons are in the even mode and $N-j$ photons are in the odd mode. Consequently, the scattering matrix $\mathbf{S}$ in the nonchiral case can be decomposed accordingly,

$$\mathbf{S} = \sum_{j=0}^{N}\mathbf{S}_{e^{(j)}}\bigotimes\mathbf{S}_{o^{(N-j)}},\tag{26}$$

where $\mathbf{S}_{e^{(j)}}$ and $\mathbf{S}_{o^{(j)}}$ are the scattering matrices for states in $\mathcal{H}_e^{\otimes j}$ and $\mathcal{H}_o^{\otimes j}$, respectively. By applying the scattering matrix onto the input state [Eq. (24)], one can directly compute the scattered states term by term in each mutually orthogonal subspace,

$$\begin{aligned}|X_{\rm out}\rangle &\equiv \mathbf{S}|X_{\rm in}\rangle\\ &= \mathbf{S}_{e^{(N)}}|X_{\rm in}\rangle_{e^{(N)}} + \mathbf{S}_{e^{(N-1)}}\bigotimes\mathbf{S}_{o^{(1)}}|X_{\rm in}\rangle_{e^{(N-1)}o^{(1)}}+\cdots\\ &\quad+\mathbf{S}_{o^{(N)}}|X_{\rm in}\rangle_{o^{(N)}}\\ &\equiv |X_{\rm out}\rangle_{e^{(N)}} + |X_{\rm out}\rangle_{e^{(N-1)}o^{(1)}}+\cdots+|X_{\rm out}\rangle_{o^{(N)}}.\end{aligned}\tag{27}$$

In the above calculations, the scattering matrices only apply to the states with the same subscripts. Using Eq. (2), each state can be transformed back into the original nonchiral system in terms of right- and left-moving photons,

$$|X_{\rm out}\rangle = |X_{\rm out}\rangle_{R^{(N)}} + |X_{\rm out}\rangle_{R^{(N-1)}L^{(1)}}+\cdots+|X_{\rm out}\rangle_{L^{(N)}}.\tag{28}$$

Here, $|X_{\rm out}\rangle_{R^{(j)}L^{(N-j)}}$ describes the scattered photon state in the $R^{(j)}L^{(N-j)}$ space where j photons propagate to the right (i.e., transmitted) and $N-j$ photons propagate to the left (reflected). Such a procedure facilitates the calculations by allocating the scattering processes into decoupled chiral systems, each of which involves less computational complexity. In the following, we demonstrate this computational scheme by calculating the scattered photon state for a three-photon Fock state.

V. EXAMPLE: THE SCATTERING OF THREE-PHOTON FOCK STATES IN NONCHIRAL SYSTEMS

A. The scattered photon wave functions

Having introduced the general approach to solve the scattering problems in the nonchiral space, we now calculate the scattered photon states for a concrete example. Consider an input state of a three-photon Fock state, formed by three overlapping photons, wherein each photon is represented by a Gaussian wave packet. Such a state is a product state which has no photonic entanglement. Each photon is on resonant with the atom and has a broad extension in the real space so that the

bandwidth is narrow. The single-photon wave function is

$$\phi_i(x) = \left(2\pi\sigma_x^2\right)^{-1/4} e^{-x^2/4\sigma_x^2} e^{i(\Omega/v)x}. \tag{29}$$

Here, $|\phi_i(x)|^2$ is normalized to unity when integrated over x from $-\infty$ to $+\infty$. The standard deviation $\sigma_x = 10v\tau_r$ and $\sigma_\omega = 0.2\Gamma$, where σ_x and σ_ω are the width of the single-photon Gaussian pulse in coordinate space and in frequency space, respectively ($\tau_r = 1/\Gamma$ is the radiation lifetime for the spontaneous emission). After scattering, the three-photon Hilbert space is decomposed into four orthogonal spaces: $R^{(3)}$, $R^{(2)}L^{(1)}$, $R^{(1)}L^{(2)}$, and $L^{(3)}$. A direct calculation using the computational scheme presented above reveals that all three photons are most likely to be reflected into the $L^{(3)}$ space, with a probability $P_{L^{(3)}} \equiv \iiint dx_1dx_2dx_3|\langle x_1,x_2,x_3|X_{\rm out}\rangle_{L^{(3)}}|^2 \approx 55\%$; while the probability that all three photons are transmitted into the $R^{(3)}$ space is the least: $P_{R^{(3)}} \equiv \iiint dx_1dx_2dx_3|\langle x_1,x_2,x_3|X_{\rm out}\rangle_{R^{(3)}}|^2 \approx 2\%$. The remaining probability is distributed within the other two possibilities with $P_{R^{(2)}L^{(1)}} \approx 13\%$ and $P_{R^{(1)}L^{(2)}} \approx 29\%$. Such a probability distribution is completely beyond the single-photon picture; for a single photon with the same Gaussian wave-function form, it is numerically found that the photon is essentially completely reflected with a reflectivity over 99% and a transmissivity less than 1% [24]. Thus, based upon the single-photon picture, *if there are no correlations induced by the atom*, one would have expected $P_{L^{(3)}} > (99\%)^3 \approx 97\%$ and $P_{R^{(3)}} < (1\%)^3 = 10^{-6}$. Thus, for the three-photon case, $P_{R^{(3)}}$ is greatly enhanced by the correlations. Such an example demonstrates that the dynamics in the multiple photon scattering processes are dramatically influenced by the correlations induced by the atom. Thus, it is of great interest to understand how the three photons get transmitted in the presence of the atom-induced correlations. For this purpose, we numerically checked the transmitted three-photon wave function in the $R^{(3)}$ space, which can be expressed as

$$\begin{aligned} h_{R^{(3)}}(x_1,x_2,x_3) = \tfrac{1}{8}[&h_{e^{(3)}}(x_1,x_2,x_3) + h_{e^{(2)}o^{(1)}}(x_1,x_2,x_3) \\ &+ h_{e^{(1)}o^{(2)}}(x_1,x_2,x_3) + h_{o^{(3)}}(x_1,x_2,x_3)]. \end{aligned} \tag{30}$$

Here, the functions $h_{e^{(3)}}(x_1,x_2,x_3)$, $h_{e^{(2)}o^{(1)}}(x_1,x_2,x_3)$, $h_{e^{(1)}o^{(2)}}(x_1,x_2,x_3)$, and $h_{o^{(3)}}(x_1,x_2,x_3)$ are the scattered wave functions in the $e^{(3)}$, $e^{(2)}o^{(1)}$, $e^{(1)}o^{(2)}$, and $o^{(3)}$ subspaces, respectively. It is numerically found that the nonchiral wave function $h_{R^{(3)}}(x_1,x_2,x_3)$ is essentially due to the chiral wave function of the three-photon bound state in $h_{e^{(3)}}(x_1,x_2,x_3)$. We emphasize that $h_{e^{(3)}}(x_1,x_2,x_3)$ also contains components other than the three-photon bound state. Specifically, it is the second term in the type-2 wave function, and the type-3 wave function that contribute to $h_{R^{(3)}}(x_1,x_2,x_3)$ (see Sec. III). In contrast, wave functions $h_{e^{(2)}o^{(1)}}$, $h_{e^{(1)}o^{(2)}}$, $h_{o^{(3)}}$, and the rest of the parts in wave functions $h_{e^{(3)}}(x_1,x_2,x_3)$ numerically cancel each other out, and thus do not contribute to the three-photon transmitted wave function $h_{R^{(3)}}(x_1,x_2,x_3)$. Therefore, we conclude that the incoming three photons, which cannot pass through the atom individually, now are able to pass through the atom as a whole by forming a three-photon bound state.

We now look into the wave functions in more detail. To facilitate the visualization of a wave function that contains three spatial coordinates, we transform the wave function in terms of the relative coordinates as follows:

$$h_r(x_1 - x_3, x_2 - x_3, x_3) \equiv \langle x_1 - x_3, x_2 - x_3, x_3|X\rangle, \tag{31}$$

where $|X\rangle$ is an arbitrary three-photon state and the subscript "r" denotes the relative coordinates $(\Delta_1,\Delta_2,x_3) \equiv (x_1 - x_3, x_2 - x_3, x_3)$. Such a transformation has a Jacobian $J = 1$, and maintains the exchange symmetry of the photonic wave function. As the transformed wave function still contains three variables, we eliminate x_3 by integrating the probability density function as follows:

$$\begin{aligned} \int dx_3|h_r(x_1 - x_3, x_2 - x_3, x_3)|^2 &\equiv \int dx_3|h_r(\Delta_1,\Delta_2,x_3)|^2 \\ &\equiv p(\Delta_1,\Delta_2). \end{aligned} \tag{32}$$

The relative probability density function $p(\Delta_1,\Delta_2)$ describes the probability density of finding two photons from the viewpoint of the third one. This function also exhibits two interesting symmetries. First, by exchanging the coordinates x_1 and x_2 in the photonic wave function h_r, one can immediately see that the function $p(\Delta_1,\Delta_2)$ is symmetric along the line $\Delta_1 = \Delta_2$, i.e.,

$$p(\Delta_1,\Delta_2) = p(\Delta_2,\Delta_1). \tag{33}$$

Secondly, $p(\Delta_1,\Delta_2)$ also exhibits inversion symmetry with respect to the origin of the coordinate system, $p(\Delta_1,\Delta_2) = p(-\Delta_1,-\Delta_2)$. The proof is straightforward:

$$\begin{aligned} &p(\Delta_1,\Delta_2) \\ &\equiv \int_{-\infty}^{+\infty} dx_3|h_r(\Delta_1,\Delta_2,x_3)|^2 \\ &= \int_{-\infty}^{+\infty} dx_3|h_r(x_1 - x_3, x_2 - x_3, x_3)|^2 \\ &= \int_{+\infty}^{-\infty} (-dx_3)|h_r[(-x_1) - (-x_3),(-x_2) - (-x_3),(-x_3)]|^2 \\ &= \int_{+\infty}^{-\infty} (-dx_3)|h_r(x_3 - x_1, x_3 - x_2, -x_3)|^2 \\ &= \int_{+\infty}^{-\infty} (-dx_3)|h_r(-\Delta_1, -\Delta_2, -x_3)|^2 \\ &= \int_{-\infty}^{+\infty} dx_3|h_r(-\Delta_1, -\Delta_2, x_3)|^2 \\ &= p(-\Delta_1, -\Delta_2). \end{aligned} \tag{34}$$

Now, we plot the relative probability density function $p_{R^{(3)}}$ and $p_{L^{(3)}}$ in the $R^{(3)}$ space and the $L^{(3)}$ space, respectively. Figure 2 plots $p_{R^{(3)}}(\Delta_1,\Delta_2)$ for the scattered three-photon state in the $R^{(3)}$ space. A pronounced single narrow peak at $\Delta_1 = \Delta_2 = 0$ clearly emerges with a full width at half maximum $\approx 1.2v\tau_r$. Thus, we have $p_{R^{(3)}}(0,\Delta_2) > p_{R^{(3)}}(\Delta_1,\Delta_2)$ for all $\Delta_1 \neq 0$. The emergence of the center peak indicates photonic bunching, as the probability of finding three photons together is significantly larger than the probability of finding them apart. Mathematically, $p_{R^{(3)}}(\Delta_1,\Delta_2)$ is related to the second-order correlation function as follows [the relation can be derived by

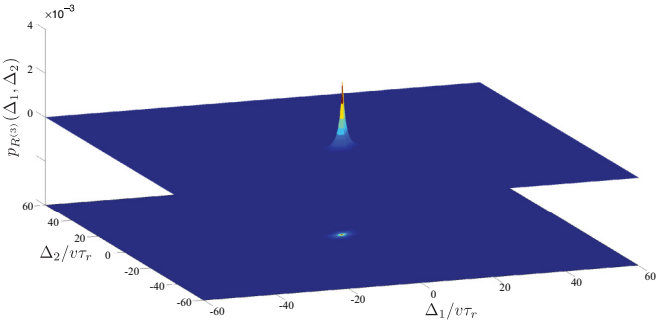

FIG. 2. (Color online) Relative probability density function $p_{R^{(3)}}(\Delta_1,\Delta_2)$ for the scattered photon states in the $R^{(3)}$ space (all three photons are transmitted and propagate to the right). A projection of the pattern is also plotted underneath to aid visualization.

using Eqs. (D12) and (32)]:

$$g^{(2)}(\tau)=\frac{2}{3}P_{R^{(3)}}\frac{\int d\Delta_2 p_{R^{(3)}}(v\tau,\Delta_2)}{\int dx_0|\phi_{R^{(3)}}(x_0)|^2|\phi_{R^{(3)}}(x_0+v\tau)|^2}. \quad (35)$$

Here, x_0 is the position of the detector, and $\phi_{R^{(3)}}(x)$ is the probability of finding a single photon at position x in the scattered state in the $R^{(3)}$ space regardless of the position of the other two photons [see Eq. (D8)]. Numerically, it is found that $\phi_{R^{(3)}}(x)$ has a similar broad extension as that of $\phi_i(x)$. τ is the difference in the arrival times between two photons. Thus, when τ is several times of τ_r, the numerator of $g^{(2)}(\tau)$ is much smaller than the numerator of $g^{(2)}(0)$ due to the pronounced peak at the center, while the denominators of $g^{(2)}(\tau)$ and $g^{(2)}(0)$ are numerically found to be roughly the same. Therefore, it is numerically found that $g^{(2)}(0)>g^{(2)}(\tau)$, confirming the photonic bunching [34].

On the other hand, the photon statistics for the reflected photons is fundamentally different in the $L^{(3)}$ space. Figure 3 plots $p_{L^{(3)}}(\Delta_1,\Delta_2)$ for the scattered three-photon photon state in the $L^{(3)}$ space, which shows six broad peaks separated by three boundaries ($\Delta_1=0$, $\Delta_2=0$, and $\Delta_1=\Delta_2$), respectively. The relative probability function is essentially depleted along the boundaries, signaling the photonic antibunching, as the probability of finding any two photons together ($\Delta_1=0$, $\Delta_2=0$, or $\Delta_1=\Delta_2$) is significantly smaller than the probability of finding them apart ($\Delta_1\neq 0$, $\Delta_2\neq 0$, and $\Delta_1\neq\Delta_2$). Mathematically, such an observation can be rigorously confirmed by directly computing the second-order correlation function for the scattered photon state in the $L^{(3)}$ space. The $g^{(2)}(\tau)$ can be similarly expressed in terms of the relative probability density function, as follows ([see Eqs. (D12) and (32)]:

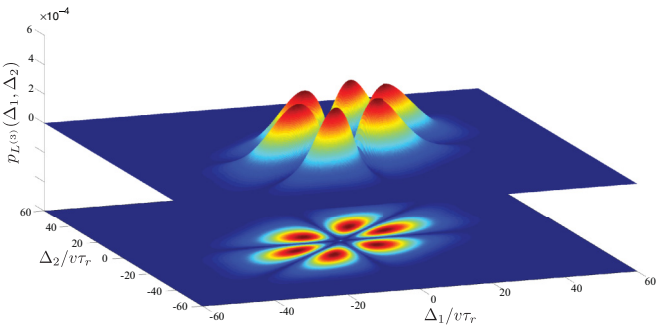

FIG. 3. (Color online) Relative probability density function $p_{L^{(3)}}(\Delta_1,\Delta_2)$ for the scattered wave function in the $L^{(3)}$ space (all three photons get reflected and propagate to the left). A projection of the pattern is also plotted underneath to aid visualization.

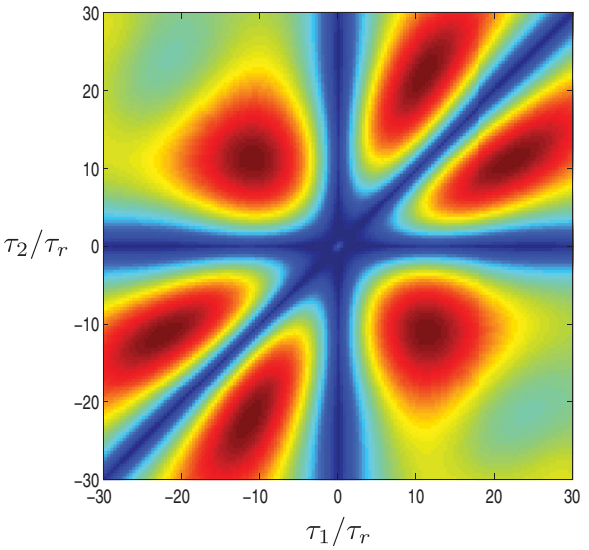

FIG. 4. (Color online) Third-order correlation function for the scattered photon wave function in the $L^{(3)}$ space.

$$g^{(2)}(\tau)=\frac{2}{3}P_{L^{(3)}}\frac{\int d\Delta_2 p_{L^{(3)}}(v\tau,\Delta_2)}{\int dx_0|\phi_{L^{(3)}}(x_0)|^2|\phi_{L^{(3)}}(x_0+v\tau)|^2}, \quad (36)$$

where $\phi_{L^{(3)}}(x)$ is the probability of finding a single photon at position x in the scattered state in the $L^{(3)}$ space regardless of the position of the other two photons, which has a similar broad extension of $\phi_i(x)$. By comparing $g^{(2)}(0)$ and $g^{(2)}(\tau)$, the prior one has a much smaller numerator and their denominators are roughly the same. Thus $g^{(2)}(0)<g^{(2)}(\tau)$, confirming photonic antibunching. Such a nonclassical phenomenon is in contrast to the bunching effect for the transmission field. Moreover, the photonic bunching and antibunching are also manifest in the states in other orthogonal spaces. For example, the two right-moving photons in the state that belongs to the $R^{(2)}L^{(1)}$ space exhibit bunching behavior, while the two left-moving photons in the state that belongs to $R^{(1)}L^{(2)}$ space exhibit antibunching behavior. We note here that the antibunching behavior has also been discussed in Refs. [35,36] when the two-level atom is driven by a weak classical driving field.

B. Third-order correlation function

From the wave functions of the scattered three-photon state, the third-order correlation function in each subspace can be computed (Appendix D). For example, the third-order correlation function for the scattered photon wave function in

the $L^{(3)}$ space is

$$g^{(3)}(\tau_1,\tau_2)=\frac{2}{9}P^2_{L^{(3)}}\frac{\int dx_0|h_{L^{(3)}}(x_0,x_0+v\tau_1,x_0+v\tau_2)|^2}{\int dx_0|\phi_{L^{(3)}}(x_0)|^2||\phi_{L^{(3)}}(x_0+v\tau_1)|^2||\phi_{L^{(3)}}(x_0+v\tau_2)|^2|}, \tag{37}$$

which is plotted in Fig. 4. At the origin of the figure, $g^{(3)}(0,0)$ is numerically found to 0.09. We found that this value could be further suppressed when the grid spacing is decreased at the expense of computational resources. Moreover, three lines $\tau_1=0$, $\tau_2=0$, and $\tau_1=\tau_2$ separate $g^{(3)}(\tau_1,\tau_2)$ into six regions. The values on the three lines are numerically found to be essentially zero. We also note that the numerator of the third-order correlation function [Eq. (37)] has the same functional form as the relative probability density function [Eq. (32)]. Thus, Fig. 4 looks qualitatively the same as that of the projection in Fig. 3. Moreover, the second-order correlation function can also be inferred from the third-order correlation as follows [the relation can be derived using Eqs. (D10) and (D11)]:

$$g^{(2)}(\tau)=\frac{3}{P_{L^{(3)}}}\int dx_3 g^{(3)}\left(\tau,\frac{x_3-x_0}{v}\right)|\phi_{L^{(3)}}(x_3)|^2. \tag{38}$$

Since $g^{(3)}(0,\tau_2)\approx 0$ essentially holds for almost all τ_2, $g^{(2)}(0)\approx 0$ is obtained. On the other hand, the third-order correlation function for the scattered photon wave function in the $R^{(3)}$ space can also be plotted, and a bright spot is observed in the origin. Such a pattern looks qualitatively the same as that of the projection in Fig. 2, and will not be duplicated here. The third-order correlation functions for the wave functions in the $R^{(2)}L^{(1)}$ and $R^{(1)}L^{(2)}$ spaces are zero, as a fixed detector can never register three photons in the current setup.

VI. CONCLUSION

In this article, we presented a comprehensive study on the analytic approach to solve the multiphoton scattering problems in a waveguide-QED system. The fermionic degree of freedom due to the atom induces photon-photon correlations through scattering processes. These photon correlations significantly modify the photon transport properties, which are completely out of the scope of the single-photon picture. For example, after the unentangled photonic Fock state scattered by the atom, the transmitted photons, due to the induced correlations, now are bunched, while the reflected photons are antibunched. Moreover, the capability of computing the scattering processes for input Fock states with an arbitrary number of photons enables one to compute the scattered state for an input coherent state. In principle, one can decompose the coherent state into a linear superposition of all possible Fock states with photon number $N=1,2,3,\ldots$. Then, the scattered photon states for all the Fock states can be computed individually. After that, all the computed scattered states are recombined to obtain the scattered state for the input coherent state. Such a possibility can be practically implemented when the mean photon number is small.

The above procedures can be further generalized to the cases when the incident photons are in the superposition state, i.e., entangled [37] or even involving photons incident from both sides of the atom. For each case, one needs to employ an appropriate input state by using corresponding operators in the first row of Eq. (23). The rest of the steps, including the construction of the **S** matrix, remain the same.

APPENDIX A: N-PHOTON FOCK STATE FOR THE CHIRAL SYSTEM: EXTENDED STATES, BOUNDED STATES, AND HYBRID STATES

In this appendix, we show the details of how to construct the eigenstates by solving Eqs. (5) and (6). To begin with, a direct observation of Eq. (5) reveals that in the region wherein none of the coordinates is zero, Eq. (5) describes a free system, thereby permitting plane wave solution. Thus, the general form of an eigenstate wave function in the region $x_1<x_2<\cdots<x_N$ can be parametrized as follows:

$$f(x_1,x_2,\ldots,x_N)=\begin{cases}\sum_{\mathcal{P}\in S_N}A_{N+1}(\mathcal{P})\exp\left(i\sum_{j=1}^{N}k_j x_{\mathcal{P}_j}\right),\\ \quad\text{in subregion } N+1\quad (x_1<x_2<\cdots<x_N<0),\\ \sum_{\mathcal{P}\in S_N}A_{N}(\mathcal{P})\exp\left(i\sum_{j=1}^{N}k_j x_{\mathcal{P}_j}\right),\\ \quad\text{in subregion } N\quad (x_1<x_2<\cdots<x_{N-1}<0<x_N),\\ \qquad\cdots\\ \qquad\cdots\\ \qquad\cdots\\ \sum_{\mathcal{P}\in S_N}A_{1}(\mathcal{P})\exp\left(i\sum_{j=1}^{N}k_j x_{\mathcal{P}_j}\right),\\ \quad\text{in subregion } 1\quad (0<x_1<x_2<\cdots<x_N).\end{cases} \tag{A1}$$

In this expression, we restrict ourselves to the region of $x_1<x_2<\cdots<x_N$, and the expressions of the wave function in other regions can be obtained using the bosonic symmetry. $k_1,k_2,\ldots,$ and k_N are in general N complex numbers subject to

the constraint of $k_1 + k_2 + \cdots + k_N = E/(v\hbar)$, among others. The orders of the k's are fixed. The summation $\mathcal{P} \in S_N$ accounts for all the $N!$ permutations of the labels $\{1,2,\ldots,N\}$, and is assigned to the coordinates x's. All the coefficients A, in addition to their explicit labels, are in general a function of all the k's and the corresponding $\mathcal{P}$. With this wave function, one can use the boundary conditions in Eqs. (5) and (6) to determine all the constraints regarding the coefficients A and wave numbers k.

To proceed, the first attempt is to assume all the k's are real and all the $N!$ A's are nonzero. To investigate those coefficient relations, we focus on two representative terms in the same subregion, which are $e^{\cdots+k_m x_j+\cdots+k_n x_{j+1}+\cdots}$ and $e^{\cdots+k_m x_{j+1}+\cdots+k_n x_j+\cdots}$ with $1 \leqslant m < n \leqslant N$ and $j = 1,2,\ldots,N-1$. Except for the exchange of x_j and x_{j+1}, these two terms have the exact same orders of the other coordinates. Specifically, we rewrite the wave function to explicitly show the two terms,

$$f(x_1,x_2,\ldots,x_N) = \begin{cases} \cdots + A_{N+1}(\ldots,j,\ldots,j+1,\ldots)e^{i(\cdots+k_m x_j+\cdots+k_n x_{j+1}+\cdots)} + \cdots \\ \cdots + A_{N+1}(\ldots,j+1,\ldots,j,\ldots)e^{i(\cdots+k_m x_{j+1}+\cdots+k_n x_j+\cdots)} + \cdots, \\ \quad \text{in subregion } N+1 \quad (x_1 < x_2 < \cdots < x_N < 0), \\ \\ \cdots + A_N(\ldots,j,\ldots,j+1,\ldots)e^{i(\cdots+k_m x_j+\cdots+k_n x_{j+1}+\cdots)} + \cdots \\ \cdots + A_N(\ldots,j+1,\ldots,j,\ldots)e^{i(\cdots+k_m x_{j+1}+\cdots+k_n x_j+\cdots)} + \cdots, \\ \quad \text{in subregion } N \quad (x_1 < x_2 < \cdots < x_{N-1} < 0 < x_N), \\ \qquad\qquad \cdots \\ \qquad\qquad \cdots \\ \qquad\qquad \cdots \\ \cdots + A_1(\ldots,j,\ldots,j+1,\ldots)e^{i(\cdots+k_m x_j+\cdots+k_n x_{j+1}+\cdots)} + \cdots \\ \cdots + A_1(\ldots,j+1,\ldots,j,\ldots)e^{i(\cdots+k_m x_{j+1}+\cdots+k_n x_j+\cdots)} + \cdots, \\ \quad \text{in subregion } 1 \quad (0 < x_1 < x_2 < \cdots < x_N). \end{cases} \tag{A2}$$

By investigating the boundary between subregion $N+1$ and subregion N where x_N crosses from 0^- to 0^+, the two equations of motion to be solved now become

$$-iv[f(x_1,x_2,\ldots,x_{N-1},0^+) - f(x_1,x_2,\ldots,x_{N-1},0^-)] + \frac{V}{\sqrt{N}}e(x_1,x_2,\ldots,x_{N-1}) = 0, \tag{A3}$$

$$iv\left[-\frac{\partial}{\partial x_1} - \frac{\partial}{\partial x_2} - \cdots - \frac{\partial}{\partial x_{N-1}} - (E/\hbar - \Omega)\right]e(x_1,x_2,\ldots,x_{N-1}) + \frac{\sqrt{N}V}{2}[f(x_1,x_2,\ldots,x_{N-1},0^+) + f(x_1,x_2,\ldots,x_{N-1},0^-)] = 0. \tag{A4}$$

By substituting Eq. (A2) into the above Eqs. (A3) and (A4), we obtain the following coefficient relations:

$$\begin{aligned} A_N(\ldots,j,\ldots,j+1,\ldots) &= \frac{k^{(x_N)} - \Omega/v - i\Gamma/(2v)}{k^{(x_N)} - \Omega/v + i\Gamma/(2v)}A_{N+1}(\ldots,j,\ldots,j+1,\ldots) = t_{k^{(x_N)}}A_{N+1}(\ldots,j,\ldots,j+1,\ldots), \\ A_N(\ldots,j+1,\ldots,j,\ldots) &= \frac{k^{(x_N)} - \Omega/v - i\Gamma/(2v)}{k^{(x_N)} - \Omega/v + i\Gamma/(2v)}A_{N+1}(\ldots,j+1,\ldots,j,\ldots) = t_{k^{(x_N)}}A_{N+1}(\ldots,j+1,\ldots,j,\ldots), \end{aligned} \tag{A5}$$

where $k^{(x_N)}$ is the k that is multiplied with x_N in the exponentials. These two equations indicate that the coefficients between the two neighboring subregions only deviate by a single-photon transmission amplitude $t_{k^{(x_N)}}$ [see Eq. (22)]. Moreover, by dividing these two equations, we get

$$\frac{A_N(\ldots,j,\ldots,j+1,\ldots)}{A_N(\ldots,j+1,\ldots,j,\ldots)} = \frac{A_{N+1}(\ldots,j,\ldots,j+1,\ldots)}{A_{N+1}(\ldots,j+1,\ldots,j,\ldots)}. \tag{A6}$$

In the following, by repeating the same procedure to other boundaries where x_{N-1}, x_{N-2}, …, and x_{j+2} cross from 0^- to 0^+ one by one, we obtain similar relations

$$\frac{A_{j+2}(\ldots,j,\ldots,j+1,\ldots)}{A_{j+2}(\ldots,j+1,\ldots,j,\ldots)} = \cdots = \frac{A_{N-1}(\ldots,j,\ldots,j+1,\ldots)}{A_{N-1}(\ldots,j+1,\ldots,j,\ldots)} = \frac{A_N(\ldots,j,\ldots,j+1,\ldots)}{A_N(\ldots,j+1,\ldots,j,\ldots)}. \tag{A7}$$

Such a relation is anticipated, as the k's associated with the coordinates that cross the boundaries are the same.

For the next boundary between subregion $j+2$ and subregion $j+1$ where x_{j+1} crosses from 0^- to 0^+, the coefficient relations between the neighboring subregions can also be computed:

$$\begin{aligned} A_{j+1}(\ldots,j,\ldots,j+1,\ldots) &= \frac{k_n-\Omega/v-i\Gamma/(2v)}{k_n-\Omega/v+i\Gamma/(2v)}A_{j+2}(\ldots,j,\ldots,j+1,\ldots) = t_{k_n}A_{j+2}(\ldots,j,\ldots,j+1,\ldots),\\ A_{j+1}(\ldots,j+1,\ldots,j,\ldots) &= \frac{k_m-\Omega/v-i\Gamma/(2v)}{k_m-\Omega/v+i\Gamma/(2v)}A_{j+2}(\ldots,j+1,\ldots,j,\ldots) = t_{k_m}A_{j+2}(\ldots,j+1,\ldots,j,\ldots). \end{aligned} \tag{A8}$$

We note that different from the previous case, this time, the k's associated with x_{j+1} are different for the two terms. Thus, Eq. (A8) does not yield the same relation that follows the rule in Eq. (A7). Moreover, the $(N-1)$-photon wave function with the photon labeled by $j+1$ being absorbed by the atom is also computed:

$$\begin{aligned} &e(x_1,x_2,\ldots,x_{j-1},x_j,x_{j+2},\ldots,x_N)\\ &= \sqrt{N}(V/v)\left[\frac{e^{i(\cdots+k_mx_j+\cdots)}}{k_n-\Omega/v+i\Gamma/(2v)}A_{j+2}(\ldots,j,\ldots,j+1,\ldots)+\frac{e^{i(\cdots+k_nx_j+\cdots)}}{k_m-\Omega/v+i\Gamma/(2v)}A_{j+2}(\ldots,j+1,\ldots,j,\ldots\cdots)\right]. \end{aligned} \tag{A9}$$

For the next boundary between subregion $N-1$ and region $N-2$ where x_j increases from 0^- to 0^+, we obtain

$$\begin{aligned} A_j(\ldots,j,\ldots,j+1,\ldots) &= \frac{k_m-\Omega/v-i\Gamma/(2v)}{k_m-\Omega/v+i\Gamma/(2v)}A_{j+1}(\ldots,j,\ldots,j+1,\ldots) = t_{k_m}A_{j+1}(\ldots,j,\ldots,j+1,\ldots),\\ A_j(\ldots,j+1,\ldots,j,\ldots) &= \frac{k_n-\Omega/v-i\Gamma/(2v)}{k_n-\Omega/v+i\Gamma/(2v)}A_{j+1}(\ldots,j+1,\ldots,j,\ldots) = t_{k_n}A_{j+1}(\ldots,j+1,\ldots,j,\ldots), \end{aligned} \tag{A10}$$

and the $(N-1)$-photon wave function with the photon labeled by j being absorbed is

$$\begin{aligned} &e(x_1,x_2,\ldots,x_{j-1},x_{j+1},x_{j+2},\ldots,x_N)\\ &= \sqrt{N}(V/v)\left[\frac{e^{i(\cdots+k_nx_{j+1}+\cdots)}}{k_m-\Omega/v+i\Gamma/(2v)}A_{j+1}(\ldots,j,\ldots,j+1,\ldots)+\frac{e^{i(\cdots+k_mx_{j+1}+\cdots)}}{k_n-\Omega/v+i\Gamma/(2v)}A_{j+1}(\ldots,j+1,\ldots,j,\ldots)\right]. \end{aligned} \tag{A11}$$

Therefore, Eqs. (A9) and (A11) represent the expressions for the $(N-1)$-photon wave function in two neighboring subregions. Since this wave function is continuous everywhere in the entire space [see Eq. (6)], the self-consistency of the function requires

$$e(x_1,x_2,\ldots,x_{j-1},0^-,x_{j+2},\ldots,x_N) = e(x_1,x_2,x_{j-1},0^+,x_{j+2},\ldots,x_N), \tag{A12}$$

which immediately leads to

$$A_{j+2}(\ldots,j,\ldots,j+1,\ldots)/A_{j+2}(\ldots,j+1,\ldots,j,\ldots) = (k_m-k_n-i\Gamma/v)/(k_m-k_n+i\Gamma/v). \tag{A13}$$

By combining Eq. (A13) with all the previous obtained coefficient relations [Eqs. (A6) and (A7)], we finally get

$$A_{N+1}(\ldots,j,\ldots,j+1,\ldots)/A_{N+1}(\ldots,j+1,\ldots,j,\ldots) = (k_m-k_n-i\Gamma/v)/(k_m-k_n+i\Gamma/v). \tag{A14}$$

It is worth mentioning here that the above analysis does not yield any restrictions on the wave numbers k. Thus, the eigenstate wave function $f(x_1,x_2,\ldots,x_N)$ is uniquely determined as

$$f(x_1,x_2,\ldots,x_N) \propto \begin{cases} \sum_{\mathcal{P}\in S_N}\left\{\prod_{m<n}[k_m-k_n-i\Gamma\,\mathrm{sgn}(\mathcal{P}_n-\mathcal{P}_m)/v]\right\}\exp\left(i\sum_{j=1}^N k_jx_{\mathcal{P}_j}\right),\\ \quad \text{in subregion } N+1 \quad (x_1<x_2<\cdots<x_N<0),\\ \qquad\cdots\\ \qquad\cdots\\ \qquad\cdots\\ \left(\prod_{j=1}^N t_{k_j}\right)\sum_{\mathcal{P}\in S_N}\left\{\prod_{m<n}[k_m-k_n-i\Gamma\,\mathrm{sgn}(\mathcal{P}_n-\mathcal{P}_m)/v]\right\}\exp\left(i\sum_{j=1}^N k_jx_{\mathcal{P}_j}\right),\\ \quad \text{in subregion } 1 \quad (0<x_1<x_2<\cdots<x_N), \end{cases} \tag{A15}$$

which describes an N-photon extended state, as each exponential term represents a free plane wave without restriction. The corresponding in-state wave function $f_{\mathrm{in}}(x_1,x_2,\ldots,x_N)$ is expressed by extending $f(x_1,x_2,\ldots,x_N)$ in subregion $N+1$ to the entire space $(-\infty<x_1,x_2,\ldots,x_N<+\infty)$,

$$f_{\mathrm{in}}(x_1,x_2,\ldots,x_N) = C_N\sum_{\mathcal{P}\in S_N}\left\{\prod_{m<n}\left[k_m-k_n-i\Gamma\,\mathrm{sgn}\left(x_{\mathcal{P}_n}-x_{\mathcal{P}_m}\right)/v\right]\right\}\exp\left(i\sum_{j=1}^N k_jx_{\mathcal{P}_j}\right), \tag{A16}$$

with normalization constant C_N to be determined. The corresponding out-state wave function $f_{\rm out}(x_1,x_2,\ldots,x_N)$, on the other hand, can be expressed by extending $f(x_1,x_2,\ldots,x_N)$ in subregion 1 to the entire space and is conveniently written as

$$f_{\rm out}(x_1,x_2,\ldots,x_N)=\left(\prod_{j=1}^{N}t_{k_j}\right)f_{\rm in}(x_1,x_2,\ldots,x_N). \tag{A17}$$

Until now, we have constructed the N-photon extended states, which are indeed the eigenstates of the Hamiltonian H_e. Nonetheless, it turns out that the N-photon extended states do not form a complete set in the N-photon Hilbert space $\mathcal{H}_e^{\otimes N}$. To find out those missing eigenstates, one needs to extend the wave numbers k into complex values. As all k's sum up to be a real number, to avoid the divergence, some of the coefficients A must be zero. The extreme case is that only one coefficient A is left to be nonzero, and all the k's are assumed to be complex numbers $\{k_j=k'_j+i\kappa_j\},\ j=1,\ldots,N$, where k'_j is the real part and κ_j is the imaginary part.

$$f(x_1,x_2,\ldots,x_N)=\begin{cases}A_{N+1}e^{i(k'_1+i\kappa_1)x_1+i(k'_2+i\kappa_2)x_2+\cdots+i(k'_N+i\kappa_N)x_N},\\ \quad\text{in subregion } N+1\quad (x_1<x_2<\cdots<x_N<0),\\ A_Ne^{i(k'_1+i\kappa_1)x_1+i(k'_2+i\kappa_2)x_2+\cdots+i(k'_N+i\kappa_N)x_N},\\ \quad\text{in subregion } N\quad (x_1<x_2<\cdots<x_{N-1}<0<x_N),\\ \qquad\cdots\\ \qquad\cdots\\ \qquad\cdots\\ A_1e^{i(k'_1+i\kappa_1)x_1+i(k'_2+i\kappa_2)x_2+\cdots+i(k'_N+i\kappa_N)x_N},\\ \quad\text{in subregion } 1\quad (0<x_1<x_2<\cdots<x_N).\end{cases} \tag{A18}$$

With this wave function, one can apply exactly the same procedures at all the boundaries to obtain all the constraints regarding the A's and k's. At the first boundary between subregion $N+1$ and subregion N where x_N crosses from 0^- to 0^+, the equations of motion yield the following coefficient relation:

$$A_N=\frac{k'_N+i\kappa_N-\Omega/v-i\Gamma/(2v)}{k'_N+i\kappa_N-\Omega/v+i\Gamma/(2v)}A_{N+1}=t_{k_N}A_{N+1}, \tag{A19}$$

which has exactly the same form as before. Moreover, the $(N-1)$-photon wave function with the photon labeled by N being absorbed is obtained accordingly:

$$e(x_1,x_2,\ldots,x_{N-1})=\sqrt{N}(V/v)\left[\frac{e^{i(k'_1+i\kappa_1)x_1+i(k'_2+i\kappa_2)x_2+\cdots+i(k'_{N-1}+i\kappa_{N-1})x_{N-1}}}{k'_N+i\kappa_N-\Omega/v+i\Gamma/(2v)}A_{N+1}\right]. \tag{A20}$$

At the next boundary between subregion N and subregion $N-1$ where x_{N-1} crosses from 0^- to 0^+, the equations of motion also yield similar coefficient relation

$$A_{N-1}=\frac{k'_{N-1}+i\kappa_{N-1}-\Omega/v-i\Gamma/(2v)}{k'_{N-1}+i\kappa_{N-1}-\Omega/v+i\Gamma/(2v)}A_N=t_{k_{N-1}}A_N, \tag{A21}$$

and the $(N-1)$-photon wave function with the photon labeled by $N-1$ being absorbed is given by

$$e(x_1,x_2,\ldots,x_{N-2},x_N)=\sqrt{N}(V/v)\left[\frac{e^{i(k'_1+i\kappa_1)x_1+i(k'_2+i\kappa_2)x_2+\cdots+i(k'_{N-2}+i\kappa_{N-2})x_{N-2}+i(k'_N+i\kappa_N)x_N}}{k'_{N-1}+i\kappa_{N-1}-\Omega/v+i\Gamma/(2v)}A_N\right]. \tag{A22}$$

Again, by applying the self-consistent condition

$$e(x_1,x_2,\ldots,x_{N-2},0^-)=e(x_1,x_2,\ldots,x_{N-2},0^+), \tag{A23}$$

we get

$$k'_{N-1}=k'_N, \tag{A24}$$

and

$$\kappa_N=\kappa_{N-1}+\Gamma/v. \tag{A25}$$

This procedure can be repeated for the rest of the boundaries, and we finally get

$$k'_N=k'_{N-1}=\cdots=k'_1\equiv k \tag{A26}$$

and

$$\kappa_N=\kappa_{N-1}+\Gamma/v=\kappa_{N-2}+2\Gamma/v=\cdots=\kappa_1+(N-1)\Gamma/v. \tag{A27}$$

As the summation of all the k's is a real number, $\kappa_1 = -(N-1)\Gamma/(2v)$. Thus, the N k's are given by

$$k_j = k + [2j - (N+1)]\Gamma/(2v), \tag{A28}$$

where $j = 1,2,\ldots,N$. With those k's, the eigenstate wave function is uniquely determined:

$$f(x_1,x_2,\ldots,x_N) \propto \begin{cases} e^{ik(x_1+x_2+\cdots+x_N)-(N-1)\Gamma(x_N-x_1)/(2v)-(N-3)\Gamma(x_{N-1}-x_2)/(2v)-\cdots}, \\ \quad \text{in subregion } N+1 \quad (x_1 < x_2 < \cdots < x_N < 0), \\ \cdots \\ \cdots \\ \cdots \\ \left(\prod_{j=1}^{N} t_{k_j}\right) e^{ik(x_1+x_2+\cdots+x_N)-(N-1)\Gamma(x_N-x_1)/(2v)-(N-3)\Gamma(x_{N-1}-x_2)/(2v)-\cdots}, \\ \quad \text{in subregion } 1 \quad (0 < x_1 < x_2 < \cdots < x_N), \end{cases} \tag{A29}$$

which describes an N-photon bound state, as the wave function is exponentially suppressed when the relative distances between any two coordinates increase. The plane wave component $e^{ik(x_1+x_2+\cdots+x_N)}$ in the wave function, on the other hand, indicates that the N-photon bound state can propagate in the entire space freely as a whole. Having constructed the N-photon bound state, its corresponding in-state wave function $f_{\text{in}}(x_1,x_2,\ldots,x_N)$ can then be obtained by extending $f(x_1,x_2,\ldots,x_N)$ in subregion $N+1$ to the entire space

$$f_{\text{in}}(x_1,x_2,\ldots,x_N) = C_N e^{ik(x_1+x_2+\cdots+x_N)-(\sum_{m<n}|x_m-x_n|)\Gamma/(2v)}, \tag{A30}$$

where C_N is the normalization constant to be determined. The out-state wave function $f_{\text{out}}(x_1,x_2,\ldots,x_N)$, on the other hand, possesses the same expression as that in Eq. (A17).

Except for the two types of eigenstates presented above, the rest of the types of eigenstates can be constructed in a similar manner by postulating different numbers of nonzero A's in the wave function. Nonetheless, most cases do not yield a solution. For those cases that do permit a valid eigenstate, the choices of the nonzero A's are unique. Thus, a unique set of k's is obtained, which in turn defines the types of eigenstates. Remarkably, it turns out that there exists a one-to-one mapping between the types of N-photon eigenstates and the partitions of the integer number N (shown in Table IV), which illustrates how many nonzero terms exist in certain types of eigenstates. For example, for $N = 4$, (2,2) is one of the partitions, and by assuming $4!/[2!2!] = 3$ nonzero terms in the wave function, we can construct the type-3 eigenstate in Table III. Also, (3,1) is another partition, and by assuming $4!/[3!1!] = 4$ nonzero terms in the wave function, we can construct the type-4 eigenstate in Table III. In general, to construct a certain type of eigenstate that corresponds to the partition $N = N_1 + N_2 + \cdots$, the number of nonzero terms in the eigenstate wave function is given by $N!/[N_1!N_2!\cdots]$.

APPENDIX B: THE NORMALIZATION FOR THE IN STATES IN THE NONCHIRAL CASE

To expand an arbitrary input state, it is convenient to normalize the in states. In this appendix, we employ the delta normalization condition to normalize the wave functions of the in states, with definitions shown as follows:

(1) One-photon case: The in-state wave function has only one specific form,

$$f_{\text{in}}^{(k)}(x) = C_1 e^{ikx}, \tag{B1}$$

where we add a superscript k to denote only one real parameter that characterizes this wave function. To normalize this wave function, we compute the overlap between two such kinds of wave functions with different superscripts,

$$\int_{-\infty}^{+\infty} dx f_{\text{in}}^{(k')*}(x) f_{\text{in}}^{(k)}(x) = |C_1|^2 2\pi\delta(k-k'), \tag{B2}$$

where the symbol $(*)$ represents the complex conjugate of the function. In the integration, the following identity is used:

$$\int_{-\infty}^{+\infty} dx\, e^{-ik'x} e^{ikx} = 2\pi\delta(k-k'). \tag{B3}$$

Thus, the normalization constant C_1 is set to be $1/\sqrt{2\pi}$ so that $f_{\text{in}}^{(k)}(x)/\sqrt{2\pi}$ is normalized to the delta function.

(2) Two-photon case: The two-photon extended state with wave function $f_{\text{in}}^{(k_1,k_2)}(x_1,x_2)$ [Eq. (12)] is characterized by two real parameters (k_1,k_2). Similarly, we compute the overlap between the wave functions with different superscripts,

$$\begin{aligned} &\int_{-\infty}^{+\infty}\int_{-\infty}^{+\infty} dx_1 dx_2 f_{\text{in}}^{(k_1',k_2')*}(x_1,x_2) f_{\text{in}}^{(k_1,k_2)}(x_1,x_2) \\ &\quad = |C_2|^2 8\pi^2[(k_1-k_2)^2 + (\Gamma/v)^2]\delta(k_1-k_1')\delta(k_2-k_2'). \end{aligned} \tag{B4}$$

To avoid double counting, we restrict $k_1 < k_2$ and $k_1' < k_2'$. Thus, the normalization constant C_2 is set to be $[(k_1-k_2)^2 + (\Gamma/v)^2]^{-1/2}/(2\sqrt{2}\pi)$.

Another type of in states to be normalized is the two-photon bound state with wave function $f_{\text{in}}^{(k)}(x_1,x_2)$ [Eq. (13)], which is characterized by only one real parameter k. A direct computation reveals that,

$$\begin{aligned} &\int_{-\infty}^{+\infty}\int_{-\infty}^{+\infty} dx_1 dx_2 f_{\text{in}}^{(k')*}(x_1,x_2) f_{\text{in}}^{(k)}(x_1,x_2) \\ &\quad = |C_2|^2 \frac{2\pi v}{\Gamma}\delta(k-k'). \end{aligned} \tag{B5}$$

Thus, $C_2 = \sqrt{\Gamma/(2\pi v)}$.

(3) Three-photon case: The first type is the three-photon extended state with wave function $f_{\text{in}}^{(k_1,k_2,k_3)}(x_1,x_2,x_3)$ [Eq. (14)], which is characterized by three real parameters (k_1,k_2,k_3).

A direct computation reveals that,

$$\int_{-\infty}^{+\infty}\int_{-\infty}^{+\infty}\int_{-\infty}^{+\infty} dx_1dx_2dx_3 f_{\rm in}^{(k_1',k_2',k_3')*}(x_1,x_2,x_3) f_{\rm in}^{(k_1,k_2,k_3)}(x_1,x_2,x_3)$$
$$= |C_3|^2 48\pi^3[(k_1-k_2)^2+(\Gamma/v)^2][(k_1-k_3)^2+(\Gamma/v)^2][(k_2-k_3)^2+(\Gamma/v)^2]\delta(k_1-k_1')\delta(k_2-k_2')\delta(k_3-k_3'), \quad \text{(B6)}$$

where we restrict $k_1<k_2<k_3$ and $k_1'<k_2'<k_3'$ to avoid double counting. Thus, C_3 is set to be $\{48\pi^3[(k_1-k_2)^2+(\Gamma/v)^2][(k_2-k_3)^2+(\Gamma/v)^2][(k_1-k_3)^2+(\Gamma/v)^2]\}^{-1/2}$.

The second type is the hybrid state $f_{\rm in}^{(k,k_3)}(x_1,x_2,x_3)$, characterized by two real parameters k and k_3, which is obtained by adding 15 other terms by permuting x_1,x_2, and x_3 in Eq. (15). Similarly, we compute the overlap between the wave functions with different superscripts:

$$\int_{-\infty}^{+\infty}\int_{-\infty}^{+\infty}\int_{-\infty}^{+\infty} dx_1dx_2dx_3 f_{\rm in}^{(k',k_3')*}(x_1,x_2,x_3) f_{\rm in}^{(k,k_3)}(x_1,x_2,x_3)$$
$$= |C_3|^2(12\pi^2 v/\Gamma)[(k-k_3)^2+[\Gamma/(2v)]^2][(k-k_3)^2+[3\Gamma/(2v)]^2]\delta(k-k')\delta(k_3-k_3')+\cdots, \quad \text{(B7)}$$

where "$\cdots$" denotes terms that contain less than two delta functions. For the normalization purpose, only the most singular term is kept. Thus, $C_3=\sqrt{\Gamma/(12\pi^2 v)}\{[(k-k_3)^2+[\Gamma/(2v)]^2][(k-k_3)^2+[3\Gamma/(2v)]^2]\}^{-1/2}$.

The third type is the three-photon bound state with wave function $f_{\rm in}^{(k)}(x_1,x_2,x_3)$ [Eq. (16)], which is characterized by only one real parameter k. A direct computation reveals that,

$$\int_{-\infty}^{+\infty}\int_{-\infty}^{+\infty} dx_1dx_2dx_3 f_{\rm in}^{(k')*}(x_1,x_2,x_3) f_{\rm in}^{(k)}(x_1,x_2,x_3) = |C_3|^2\frac{\pi v^2}{\Gamma^2}\delta(k-k'). \quad \text{(B8)}$$

Thus, $C_3=\Gamma/(v\sqrt{\pi})$.

(4) N-photon case: The wave function of the N-photon extended state is $f_{\rm in}^{(k_1,k_2,\ldots,k_N)}(x_1,x_2,\ldots,x_N)$ [Eq. (17)], which is characterized by N real parameters $(k_1,k_2,\ldots,k_N)$. A direct computation reveals that ($k_1<k_2<\cdots<k_N$ and $k_1'<k_2'<\cdots<k_N'$ are restricted to avoid double counting),

$$\int_{-\infty}^{+\infty}\cdots\int_{-\infty}^{+\infty} dx_1dx_2\cdots dx_N f_{\rm in}^{(k_1',k_2',\ldots,k_N')*}(x_1,x_2,\ldots,x_N) f_{\rm in}^{(k_1,k_2,\ldots,k_N)}(x_1,x_2,\ldots,x_N)$$
$$= |C_N|^2\left\{\prod_{m<n}[(k_m-k_n)^2+(\Gamma/v)^2]\right\}N!(2\pi)^N\delta(k_1-k_1')\delta(k_2-k_2')\cdots\delta(k_N-k_N'). \quad \text{(B9)}$$

Thus, $C_N=\{\prod_{m<n}[(k_m-k_n)^2+(\Gamma/v)^2]\}^{-1/2}/(\sqrt{N!(2\pi)^N}$. In contrast, the wave function of the N-photon bound state $f_{\rm in}^{(k)}(x_1,x_2,\ldots,x_N)$ [Eq. (19)], which is characterized by only one real parameter k. A direct computation reveals that,

$$\int_{-\infty}^{+\infty}\cdots\int_{-\infty}^{+\infty} dx_1dx_2\cdots dx_N f_{\rm in}^{(k')*}(x_1,x_2,\ldots,x_N) f_{\rm in}^{(k)}(x_1,x_2,\ldots,x_N) = |C_N|^2\frac{2\pi}{(N-1)!(\Gamma/v)^{N-1}}\delta(k-k'). \quad \text{(B10)}$$

Thus, $C_N=\sqrt{(N-1)!(\Gamma/v)^{N-1}/(2\pi)}$. The normalization constants for other hybrid states can be determined through a similar procedure.

APPENDIX C: COMPLETENESS CHECK

The construction of the scattering matrix relies on the the completeness of the set of in states $\{|{\rm in}\rangle\}$ in the chiral space. In the chiral space, the completeness condition is expressed as the following identity:

$$\sum_j\sum_{\{k\}}\left|{\rm in}_j^{\{k\}}\right\rangle\left\langle{\rm in}_j^{\{k\}}\right| = \mathbb{1}, \quad \text{(C1)}$$

where the subscript $j=1,2,\ldots,Z(N)$ accounts for all the types of the in states and the set $\{k\}$ is for all the possible k's in a given type. In this appendix, we provide a numerical check for the completeness for the chiral case; that is, we will check if the equality in Eq. (C1) holds. This procedure can be straightforwardly generalized to the nonchiral case without further conceptual difficulties.

As all the in states are given in real-space forms, we first project an arbitrary N-photon state $|X\rangle$ into the real space, which is also chosen to be normalized as

$$\int\cdots\int dx_1\cdots dx_N|\langle x_1,\ldots,x_N|X\rangle|^2 = 1. \quad \text{(C2)}$$

Then, by inserting the to-be-checked Eq. (C1) into Eq. (C2), we get

$$\sum_j P_j \stackrel{?}{=} 1, \quad \text{(C3)}$$

where

$$P_j \equiv \sum_{\{k\}}\int\cdots\int dx_1\cdots dx_N\left|\langle x_1,\ldots,x_N|{\rm in}_j^{\{k\}}\rangle\langle{\rm in}_j^{\{k\}}|X\rangle\right|^2, \quad \text{(C4)}$$

TABLE V. Completeness check for in states in $\mathcal{H}_e^{\otimes 3}$. To ease the computational burden, for the purpose of checking completeness, σ_x is smaller than that used in previous section, where a much larger σ_x is required for near single frequency condition.

$\sigma_x/v\tau_r$	P_1	P_2	P_3	Summation
0.5	0.008	0.052	0.941	1.001
1	0.017	0.163	0.821	1.001
2	0.033	0.566	0.393	0.992

describing the weight of $|X\rangle$ in the jth type in states. When writing down Eqs. (C3) and (C4), we have used the fact that the in states with different j and set $\{k\}$ are orthogonal with each other. The orthogonality can either be proved by standard procedures or directly be checked numerically.

As a concrete example, we numerically check the in states in $\mathcal{H}_e^{\otimes 3}$. The incoming three-photon Fock state $|X\rangle$ is assumed to be three identical and overlapping Gaussian wave packets, characterized by standard deviation σ_x. Table V lists all the P_j's for varying σ_x. As we can see from the table, for all σ_x investigated, the summations of all the P_j's are very close to unity, with relative error less than 1%. Such a result numerically confirms both the completeness and orthogonality of the three-photon in states in $\mathcal{H}_e^{\otimes 3}$.

APPENDIX D: THE PHOTON CORRELATIONS OF ARBITRARY ORDER

The second-order photon correlation function, which is the primary quantity to describe the statistical properties of a stream of photons, is defined as [38]

$$g^{(2)}(x_0,t,t+\tau)=\frac{\langle E^-(x_0,t)E^-(x_0,t+\tau)E^+(x_0,t+\tau)E^+(x_0,t)\rangle}{\langle E^-(x_0,t)E^+(x_0,t)\rangle\langle E^-(x_0,t+\tau)E^+(x_0,t+\tau)\rangle}, \tag{D1}$$

where $\langle\cdot\rangle$ is the expectation value of a normalized state, and $E^-(x_0,t)$ and $E^+(x_0,t)$ are the positive and negative frequency components, respectively, of the electric field operators. t and $t+\tau$ are the two times to make the measurements and x_0 is the position of the detector. By using the real-space approach presented above, it can be shown that the second-order correlation function can be reduced to [39]

$$g_i^{(2)}(\tau)=\frac{\langle C_i^\dagger(x_0)C_i^\dagger(x_0+v\tau)C_i(x_0+v\tau)C_i(x_0)\rangle}{\langle C_i^\dagger(x_0)C_i(x_0)\rangle\langle C_i^\dagger(x_0+v\tau)C_i(x_0+v\tau)\rangle}, \tag{D2}$$

where $i=R$ or L represents the measurements for the right-moving photons or the left-moving photons, respectively. For incoming photons from the left, if $x_0>0$, the detector is placed on the transmitted side, which only registers the right-moving photons in the transmitted scattered state; on the other hand, if $x_0<0$, the detector is placed on the reflected side, which registers the right-moving photons in the input state and the left-moving photons in the reflected scattered state. In principle, the correlation function does not depend on the placement of the detector, i.e., x_0. Analytically, we found out it is indeed so; numerically, we found there exists a very minute difference. For brevity, hereafter, we drop the subscript "i" in the correlation function.

Equation (D2) can be further expressed in terms of the wave function of the transmitted or reflected part of the scattered state. For example, the second-order correlation function for a two-photon state, now takes the following form:

$$g^{(2)}(\tau)=\frac{1}{2}\left[\iint dx_1dx_2|h(x_1,x_2)|^2\right]\frac{|h(x_0,x_0+v\tau)|^2}{\left[\int dx_2|h(x_0,x_2)|^2\right]\left[\int dx_1|h(x_1,x_0+v\tau)|^2\right]}, \tag{D3}$$

where $h(x_1,x_2)$ is the two-photon wave function of the relevant state. Using a similar approach, the second-order correlation function for a three-photon state can also be written as

$$g^{(2)}(\tau)=\frac{2}{3}\left[\iiint dx_1dx_2dx_3|h(x_1,x_2,x_3)|^2\right]\frac{\int dx_3|h(x_0,x_0+v\tau,x_3)|^2}{\left[\iint dx_2dx_3|h(x_0,x_2,x_3)|^2\right]\left[\int\int dx_1dx_3|h(x_1,x_0+v\tau,x_3)|^2\right]}, \tag{D4}$$

where $h(x_1,x_2,x_3)$ is the three-photon wave function of the relevant state. Such a procedure can be further generalized to the N-photon state, and its second-order correlation function is

$$\begin{aligned}g^{(2)}(\tau)=&\frac{N-1}{N}\left[\int\cdots\int dx_1\cdots dx_N|h(x_1,x_2,\ldots,x_N)|^2\right]\\&\times\frac{\int\cdots\int dx_3\cdots dx_N|h(x_0,x_0+v\tau,x_3,\ldots,x_N)|^2}{\left[\int\cdots\int dx_2\cdots dx_N|h(x_0,x_2,\ldots,x_N)|^2\right]\left[\int\cdots\int dx_1dx_3\cdots dx_N|h(x_1,x_0+v\tau,x_3,\ldots,x_N)|^2\right]},\end{aligned} \tag{D5}$$

where $h(x_1,x_2,\ldots,x_N)$ is the N-photon wave function of the relevant state.

Moreover, the higher-order correlation functions can also be obtained in a similar manner. For example, the third-order correlation function for a three-photon state is

$$g^{(3)}(\tau_1,\tau_2) = \frac{2}{9}\left[\iiint dx_1dx_2dx_3|h(x_1,x_2,x_3)|^2\right]^2 \times \frac{|h(x_0,x_0+v\tau_1,x_0+v\tau_2)|^2}{\left[\iint dx_2dx_3|h(x_0,x_2,x_3)|^2\right]\left[\iint dx_1dx_3|h_i(x_1,x_0+v\tau_1,x_3)|^2\right]\left[\iint dx_1dx_2|h(x_1,x_2,x_0+v\tau_2)|^2\right]}, \tag{D6}$$

where τ_1 and τ_2 are the differences of the three arrival times of the photons. Similarly, the mth-order correlation function for an N-photon state ($m \leqslant N$) is

$$g^{(m)}(\tau_1,\ldots,\tau_{m-1}) = \frac{N!}{(N-m)!N^m}\left[\int\cdots\int dx_1\cdots dx_N|h(x_1,x_2,\ldots,x_N)|^2\right]^{m-1} \times \frac{\int\cdots\int dx_{m+1}\cdots dx_N|h(x_0,x_0+v\tau_1,x_0+v\tau_2,\ldots,x_0+v\tau_{m-1},x_{m+1},\ldots,x_N)|^2}{\left[\int\cdots\int dx_2\cdots dx_N|h(x_0,x_2,\ldots,x_N)|^2\right]\cdots\left[\int\cdots\int dx_1\cdots dx_{m-1}dx_{m+1}\cdots dx_N|h(x_1,\ldots,x_{m-1},x_0+v\tau_{m-1},x_{m+1},\ldots,x_N)|^2\right]}, \tag{D7}$$

where $\tau_1,\tau_2,\ldots,\tau_{m-1}$ are differences of the m arrival times of the photons.

Among all the correlation functions presented above, the second- and third-order correlation functions for the three-photon state are of particular interest and discussed in Sec. V. To simplify the expressions, one can define

$$|\phi(x)|^2 \equiv \iint dx_2dx_3|h(x,x_2,x_3)|^2, \tag{D8}$$

and

$$P \equiv \iiint dx_1dx_2dx_3|h(x_1,x_2,x_3)|^2 = \int dx_1|\phi(x_1)|^2. \tag{D9}$$

The first quantity $|\phi(x)|^2$ describes the probability of finding one photon at position x regardless of the positions of the other two photons. The second quantity P is the total probability of the three-photon state in the entire space. Thus, the correlation functions can be further simplified as

$$g^{(2)}(\tau) = \frac{2}{3}P\frac{\int dx_3|h(x_0,x_0+v\tau,x_3)|^2}{|\phi(x_0)|^2|\phi(x_0+v\tau)|^2}, \tag{D10}$$

and

$$g^{(3)}(\tau_1,\tau_2) = \frac{2}{9}P^2\frac{|h(x_0,x_0+v\tau_1,x_0+v\tau_2)|^2}{|\phi(x_0)|^2||\phi(x_0+v\tau_1)|^2||\phi(x_0+v\tau_2)|^2|}. \tag{D11}$$

Numerically, we found that the above exact expressions can be computationally extensive when small denominators are present, which occur when $|\phi(x)|^2$ is small (e.g., at the edge of the wave packet). To ease the computational expense, we perform the following trick by integration over x_0 for both numerators and denominators independently (note the analytic result is independent of x_0). Such a procedure numerically gets away with the small denominator problem, and results in the following expressions used in the article:

$$g^{(2)}(\tau) = \frac{2}{3}P\frac{\iint dx_0dx_3|h(x_0,x_0+v\tau,x_3)|^2}{\int dx_0|\phi(x_0)|^2|\phi(x_0+v\tau)|^2}, \tag{D12}$$

and

$$g^{(3)}(\tau_1,\tau_2) = \frac{2}{9}P^2\frac{\int dx_0|h(x_0,x_0+v\tau_1,x_0+v\tau_2)|^2}{\int dx_0|\phi(x_0)|^2|\phi(x_0+v\tau_1)|^2|\phi(x_0+v\tau_2)|^2}. \tag{D13}$$

[1] M. Hofheinz, E. M. Weig, M. Ansmann, R. C. Bialczak, E. Lucero, M. Neeley, A. D. Oconnell, H. Wang, J. M. Martinis, and A. N. Cleland, Generation of Fock states in a superconducting quantum circuit, Nature (London) **454**, 310 (2008).

[2] J. Jacabson, G. Björk, I. Chuang, and Y. Yamamoto, Photonic de Broglie Waves, Phys. Rev. Lett. **74**, 4835 (1995).

[3] A. N. Boto, P. Kok, D. S. Abrams, S. L. Braunstein, C. P. Williams, and J. P. Dowling, Quantum Interferometric Optical Lithography: Exploiting Entanglement to Beat the Diffraction Limit, Phys. Rev. Lett. **85**, 2733 (2000).

[4] S. Bentley and R. Boyd, Nonlinear optical lithography with ultra-high sub-Rayleigh resolution, Opt. Express **12**, 5735 (2004).

[5] M. Tsang, Quantum Imaging Beyond the Diffraction Limit by Optical Centroid Measurements, Phys. Rev. Lett. **102**, 253601 (2009).

[6] V. Giovannetti, S. Lloyd, L. Maccone, and J. H. Shapiro, Sub-Rayleigh-diffraction-bound quantum imaging, Phys. Rev. A **79**, 013827 (2009).

[7] C. Monroe, Quantum information processing with atoms and photons, Nature (London) **416**, 238 (2002).

[8] A. Kuhn, M. Hennrich, and G. Rempe, Deterministic Single-Photon Source for Distributed Quantum Networking, Phys. Rev. Lett. **89**, 067901 (2002).

[9] V. I. Rupasov and V. I. Yudson, Rigorous theory of cooperative spontaneous emission of radiation from a lumped system of two-level atoms: Bethe ansatz method, Zh. Eksp. Teor. Fiz. **87**, 1617 (1984).

[10] J.-T. Shen and S. Fan, Strongly Correlated Two-Photon Transport in a One-Dimensional Waveguide Coupled to a Two-Level System, Phys. Rev. Lett. **98**, 153003 (2007).

[11] J. T. Shen and S. Fan, Strongly correlated multiparticle transport in one dimension through a quantum impurity, Phys. Rev. A **76**, 062709 (2007).

[12] J. Daboul and M. M. Nieto, Quantum bound states with zero binding energy, Phys. Lett. A **190**, 357 (1994).

[13] K. Hennessy, A. Badolato, M. Winger, D. Gerace, M. Atatüre, S. Gulde, S. Fält, E. L. Hu, and A. Imamoğlu, Quantum nature of a strongly coupled single quantum dot–cavity system, Nature (London) **445**, 896 (2007).

[14] I. Fushman, D. Englund, A. Faraon, N. Stoltz, P. Petroff, and J. Vučković, Controlled phase shifts with a single quantum dot, Science **320**, 769 (2008).

[15] J. You and F. Nori, Atomic physics and quantum optics using superconducting circuits, Nature (London) **474**, 589 (2011).

[16] A. Wallraff, D. I. Schuster, A. Blais, L. Frunzio, R. Huang, J. Majer, S. Kumar, S. M. Girvin, and R. J. Schoelkopf, Strong coupling of a single photon to a superconducting qubit using circuit quantum electrodynamics, Nature (London) **431**, 162 (2004).

[17] N. B. Manson, J. P. Harrison, and M. J. Sellars, Nitrogen-vacancy center in diamond: Model of the electronic structure and associated dynamics, Phys. Rev. B **74**, 104303 (2006).

[18] J. Eschner, C. Raab, F. Schmidt-Kaler, and R. Blatt, Light interference from single atoms and their mirror images, Nature (London) **413**, 495 (2001).

[19] C. J. Hood, M. S. Chapman, T. W. Lynn, and H. J. Kimble, Real-Time Cavity QED with Single Atoms, Phys. Rev. Lett. **80**, 4157 (1998).

[20] M. Tokushima, H. Kosaka, A. Tomita, and H. Yamada, Light-wave propagation through a 120 sharply bent single-line-defect photonic crystal waveguide, Appl. Phys. Lett. **76**, 952 (2000).

[21] T. Lund-Hansen, S. Stobbe, B. Julsgaard, H. Thyrrestrup, T. Sünner, M. Kamp, A. Forchel, and P. Lodahl, Experimental Realization of Highly Efficient Broadband Coupling of Single Quantum Dots to a Photonic Crystal Waveguide, Phys. Rev. Lett. **101**, 113903 (2008).

[22] V. S. C. M. Rao and S. Hughes, Single quantum-dot Purcell factor and β factor in a photonic crystal waveguide, Phys. Rev. B **75**, 205437 (2007).

[23] K. K. Y. Lee, Y. Avniel, and S. G. Johnson, Design strategies and rigorous conditions for single-polarization single-mode waveguides, Opt. Express **16**, 15170 (2008).

[24] J. T. Shen and S. Fan, Coherent photon transport from spontaneous emission in one-dimensional waveguides, Opt. Lett. **30**, 2001 (2005).

[25] J.-T. Shen and S. Fan, Theory of single-photon transport in a single-mode waveguide. I. Coupling to a cavity containing a two-level atom, Phys. Rev. A **79**, 023837 (2009).

[26] F. D. M. Haldane and S. Raghu, Possible Realization of Directional Optical Waveguides in Photonic Crystals with Broken Time-Reversal Symmetry, Phys. Rev. Lett. **100**, 013904 (2008).

[27] Z. Wang, Y. D. Chong, J. Joannopoulos, and M. Soljačić, Reflection-Free One-Way Edge Modes in a Gyromagnetic Photonic Crystal, Phys. Rev. Lett. **100**, 013905 (2008).

[28] W. Greiner and J. Reinhardt, *Field Quantization* (Springer, New York, 1996).

[29] J. J. Sakurai, *Modern Quantum Mechanics* (Addison-Wesley, Reading, MA, 1994).

[30] K. C. Obi and J.-T. Shen, Perturbative and iterative methods for photon transport in one-dimensional waveguides, Opt. Commun. **343**, 135 (2015).

[31] M. Karbach and G. Muller, Introduction to the Bethe Ansatz I, arXiv:cond-mat/9809162.

[32] G. H. Hardy and S. Ramanujan, Asymptotic formulæ in combinatory analysis, Proc. London Math. Soc. **2**, 75 (1918).

[33] H. Zheng, D. J. Gauthier, and H. U. Baranger, Waveguide QED: Many-body bound-state effects in coherent and Fock-state scattering from a two-level system, Phys. Rev. A **82**, 063816 (2010).

[34] L. Mandel and E. Wolf, *Optical Coherence and Quantum Optics* (Cambridge University Press, Cambridge, 1995).

[35] H. J. Kimble, M. Dagenasis, and L. Mandel, Photon Antibunching in Resonance Fluorescence, Phys. Rev. Lett. **39**, 691 (1977).

[36] J. T. Höffges, H. W. Baldauf, T. Eichler, S. R. Helmfrid, and H. Walther, Heterodyne measurement of the fluorescent radiation of a single trapped ion, Opt. Commun. **133**, 170 (1997).

[37] M. Bradford and J. T. Shen, Single-photon frequency conversion by exploiting quantum interference, Phys. Rev. A **85**, 043814 (2012).

[38] M. Scully and M. Zubairy, *Quantum Optics* (Cambridge University Press, Cambridge, 1997).

[39] M. Bradford and J. T. Shen, Numerical approach to statistical properties of resonance fluorescence, Opt. Lett. **39**, 5558 (2014).